Efficient Carbon Recycling at the Central-Northern Lesser Antilles Arc: Implications to deep carbon recycling in global subduction zones

Authors: Kan Li[1,*], Long Li[1], Cyril Aubaud[2], Karlis Muehlenbachs[1]

Affiliations:

[1]Department of Earth and Atmospheric Sciences, University of Alberta, Edmonton, Alberta, Canada.

[2]Laboratoire de Geochimie des Isotopes Stables, Institut de Physique du Globe, Université de Paris, France

Corresponding author: Kan Li (kan3@ualberta.ca)

Key Points:

- Subducting input and volcanic output fluxes of carbon at the Central-Northern Lesser Antilles arc were constrained by instrumental data.
- Comparison shows that slab carbon is efficiently recycled through volcanic emissions at this subduction zone
- This implies little carbon loss at the fore-arc region as well as little carbon subduction into the deep mantle in this individual subduction zone.

ABSTRACT:

Carbon recycling efficiency of arc (CREA) is an important parameter to assess the recycling of slab carbon into Earth's deep interior. Although previous studies observed variable degrees of recycled slab carbon at global arcs, the CREA value of any individual subduction zone has not been obtained due to the loose constraints on carbon budget in altered oceanic crust (AOC). Here, through estimates of carbon input by both sediments and AOC at DSDP Site 543 and recycled carbon output from major volcanoes in the Central-Northern Lesser Antilles, we show an extremely efficient carbon recycling case, with the CREA value reaching $100^{\pm 27}$%. Nearly complete slab carbon release at sub-arc depth implies little carbon has been lost in the forearc region or subducted into the deep mantle in this subduction zone. Our results highlight strongly variable CREA on a global scale, which must be considered in the modeling of global deep carbon cycle.

Plain Language Summary

Subduction zones are the major channel to deliver crustal carbon into the mantle. However, the fate of crustal carbon at a variety of depth (e.g., forearc, sub-arc, beyond arc) in the subduction channel is poorly quantified, which is an obstacle to our understanding of the deep carbon cycle. Here, we assessed the carbon recycling efficiency in the Central-Northern Lesser Antilles arc by comparing the carbon input flux (estimated from data of the subducting slab recovered by DSDP drillings) with carbon output flux (estimated based of volcanic emission data). We found that the subducted crustal carbon was nearly completely recycled by arc volcanism in the Central-Northern Lesser Antilles. This implies little carbon loss within the forearc region and little carbon subducted into the deep mantle in the Central-Northern Lesser Antilles, which differs from some other subduction zones (e.g., the Izu-Bonin-Mariana and Central America) that show low carbon recycling efficiencies. Our discovery highlights that the carbon recycling in subduction zone is highly variable on a global scale.

Keywords: Lesser Antilles; volcanic emission; subduction; efficient carbon recycling

1. Introduction

Arc volcanism is a crucial pathway to recycle the fixed carbon in the subducting slab back to the atmosphere (e.g., Fisher et al., 2019; Hilton et al., 2002). Several mechanisms, including de-carbonation (e.g., Cook-Kollars et al., 2014; Gorman et al., 2006), carbonate dissolution (e.g., Ague & Nicolescu, 2014; Frezzotti et al., 2011; Kelemen & Manning, 2015), diapiric flow (e.g., Behn et al., 2011; Marschall & Schumacher, 2012), and partial melting (e.g., Martin & Hermann, 2018) have been proposed to be able to mobilize carbon out of subducting slab within the forearc and sub-arc regions. Meanwhile, some carbon stabilization mechanisms, such as re-carbonation (Piccoli et al., 2016; Scambelluri et al., 2016) and carbonate reduction (Galvez et al., 2013), have also been proposed to enable deep carbon subduction. Previous modeling or experimental studies looking into the effect of individual or combined carbon mobilizing mechanisms gave very different results in term of the survival of slab carbon beyond arc depth (e.g., Collins et al., 2015; Gorce et al., 2019; Gorman et al., 2006; Kelemen & Manning, 2015; Kerrick & Connolly, 2001a, 2001b). The integrated effect of both carbon mobilizing and stabilizing processes on subduction-zone carbon recycling appears too complicated to be constrained by either modeling or experimental simulations. Therefore, comparison between carbon input flux into the trench and recycled carbon output flux from arc volcanoes is by far the most straightforward way to assess deep carbon recycling (e.g., De Leeuw et al., 2007; Li & Bebout, 2005; Shaw et al., 2003). Carbon recycling efficiency at arcs (CREA), which is defined as the percentage of subducted slab carbon that is recycled by arc volcanism, quantifies the carbon returned to the surface or carried downward beyond the sub-arc depth to the deeper mantle.

By comparison of carbon budgets in subducting sediments and emitted volcanic gases, previous studies have shown that slab carbon being recycled through arcs is highly variable on a global scale, e.g., the recycled carbon released from arc accounts for small amounts of slab carbon (equivalent to 12-29% of sedimentary carbon) in the Central American margin (De Leeuw et al., 2007), but significantly higher (even larger than the subducting sedimentary carbon) in the Sunda margin (House et al., 2019). One important gap in these studies is that the carbon inventory in altered oceanic crust (AOC), a key carbon reservoir in subducting slab (Li et al., 2019), had not been well constrained, and thus was not included in those previous quantifications for carbon recycling in these subduction zones. Some early efforts (e.g., Hilton et al., 2002; Johnston et al.,

2011) assumed a mean CO_2 content of 0.2wt.% (Alt & Teagle, 1999) and a constant thickness (7 km) for global AOC to estimate the CREA values of world's major subduction zones. However, a recent study (Li et al., 2019) suggested that the carbon content and effective depth of AOC sections that contain carbon are highly variable in global AOCs and thus constant values cannot be applied.

Here, using the relatively well studied Lesser Antilles subduction zone as an example, we provide the first study of the carbon contents and isotopic compositions in a full spectrum of carbon reservoirs in a subducting slab (i.e., organic carbon and carbonate in both sediment and AOC; see Supporting Information Text S1 for detailed method). These data are then integrated with previously published volcanic emission data to calculate the carbon input and output fluxes, aiming to estimate the CREA value in the Central-Northern Lesser Antilles (C-N LA) subduction zone. The C-N LA margin is particular of interests to study because, in contrast to the other two intensively studied convergent margins (i.e., Izu-Bonin-Mariana and Central America) which represent the relatively few subducting slabs that contain abundant sedimentary carbonate (House et al., 2019; Li & Bebout, 2005; Plank et al., 2007), the C-N LA subducting slab has carbonate-poor sediments, and thus can supplement previous studies to provide more insights into the understanding of the deep carbon cycle on a global scale.

2. Geological Background

The 850 km LA arc chain comprises a number of intra-oceanic volcanoes (Fig. 1). They were produced by the westward subduction of the Atlantic oceanic lithosphere underneath the Caribbean Plate, with an ultra-slow convergence rate of 24 mm/yr (Jarrard, 2003). The recent LA arc chain has been active since the late Chattian (24.8-19 Ma) (Bouysse et al., 1990; Germa et al., 2011) and can be divided into three segments. The northern part spreads for 160 km from Nevis to Saba, the central part is about 330 km from Martinique to Montserrat, and the southern part extends for 360 km from Grenada to St. Lucia (Fig.1) (each length was read from GeoMapApp; http://www.geomapapp.org). Currently, the most active volcanoes with major magmatic eruptions in the C-N LA arc include the Soufriere Hills Volcano in Montserrat, the La Soufriere Volcano in Guadeloupe, Mount Pelée Volcano in Martinique.

The LA arc chain has been a focused site for the study of slab recycling and crust-mantle interaction (e.g., Bezard et al., 2014; Carpentier et al., 2008; Labanieh et al., 2010; Van Soest et al., 1998). This is mainly benefited from the two drill cores by the Deep Sea Drilling Program (DSDP) recovering subducting material in the north (Site 543, 260 km east of Dominica; Fig. 1) and the south (Site 144, 800 km southeast of Grenada) of the LA trench, which provide key reference data for the discussion on slab contribution (e.g., Carpentier et al., 2008; Labanieh et al., 2010) and potential crustal contamination (e.g., Bezard et al., 2014, 2015; Devine & Sigurdsson, 1980; Van Soest et al., 1998) in the LA arc.

Comparison between DSDP Sites 543 and 144 indicates that the stratigraphy of subducting sediments changes significantly from the north to the south along the LA trench. Sediments in DSDP Hole 543 consist mainly of pelagic and radiolarian clays (Shipboard Scientific Party, 1984; Fig. 2), which are considered to represent the material entering the C-N LA trench (Martinique to Saba). Sediments in Hole 144 are rich in carbonate (Shipboard scientific Party, 1972), which are more representative of the material entering the southern LA trench. While upper part of the seafloor sediments has been accreted all along the LA trench, the décollement has been only identified at Site 543 at171 meters below the seafloor (Shipboard Scientific Party, 1984; Fig.2), but has not been identified at Site 144. Since the décollement depth is a key parameter to determine the input carbon flux, although we report the carbon content and isotopic data for both Site 543 and Site 144 (Table S1-S5 in the Supplementary Information or SI; Fig. 2 and SI - Fig. S1), our modeling of carbon input flux and related discussion will be based on Site 543 samples and thus more appropriate to be applied to the C-N LA arc.

3. Estimate of Carbon Input and Output Fluxes

The carbon input into the C-N LA trench is mainly contributed by subducting sediments and AOC, which is modelled in detail below.

3.1 Sedimentary Carbon Input

In the sediments below the décollement at Site 543, carbonate mainly concentrates in a ~32-meter-thick layer (Unit 6; Fig. 2) with calcareous ferruginous claystone (Wright., 1984). The concentrations of carbonate carbon vary from 0 ppm to 63840 ppm with a weighted average value of 4157 ppm (Wright., 1984; Fig. 2, SI - Table S1). The $\delta^{13}C$ values of carbonate were only

measured for two samples in Unit 6 (see SI - Text S1 for methods, and Fig. 2 and Table S2 for data), which gave a weighted average value of 2.0‰ (Fig. 2 and Table S1). The concentrations of organic carbon in the sediments below the décollement vary from 219 ppm to 1464 ppm with a weighted average value of 720 ppm (see SI - Text S1 for methods, and Fig. 2 and Table S2 for data). The $\delta^{13}C$ values of organic carbon range from -23.3‰ to -26.0‰ with a weighted average value of -24.4‰ (Fig. 2; Table S2). Employing the same method by Li and Bebout (2005) using the concentrations of organic and carbonate carbon (Fig.2; Table S1 and S2) and the dry density (Shipboard Scientific Party, 1984) of the sediment sections, convergence rate (24 mm/yr), and the length of the C-N LA trench, the subducting carbonate and organic carbon fluxes (in the sediments below the décollement) were estimated to be 1.03×10^9 mol/yr and 1.82×10^8 mol/yr, respectively. All together, we obtained a total carbon input flux of 1.21×10^9 mol/yr with a weighted average $\delta^{13}C$ value of -2.0‰ for sediments subducting into the C-N LA trench.

3.2 AOC Carbon Input

To estimate the carbon input flux contributed by AOC, we employed the same method by Li et al. (2019). Because most of carbon (either inorganic or organic) in AOC was incorporated during low-temperature alteration, only the AOC section above the 100 ºC isotherm was considered in the modeling (Li et al., 2019). Based on the Simple Plate Cooling model (Stein & Stein, 1992), the 100 ºC isotherm in the AOC section before the LA trench lies at 3393^{+377}_{-309} meters below the sediment-basement interface (see SI - Text S2 and Li et al., 2019 for detailed modeling). To calculate the carbon inventory in this 3393-meter AOC section, we adopted a standard stratigraphy employed by previous studies (e.g., Alt & Teagle, 1999; Kelemen & Manning, 2015) including 5 lithologic stratums, i.e., from top to bottom, 300-meter upper volcanics, 300-meter lower volcanics, 200-meter transition zone, 1,200-meter sheeted dikes, and the rest as gabbro.

The carbon inventory of the upper volcanics can be constrained by the 44-meter Campanian (~87 Ma) volcanics recovered from Hole 543A (Shipboard Scientific Party, 1984), which are slightly to moderately altered and characterized by background alteration without obvious carbonate veins (see Li et al., 2019 for detailed sample description). Thirteen samples from DSDP Hole 543A were analyzed for this study. The concentrations of disseminated carbonate carbon

vary from 19 ppm to 9,175 ppm with a weighted average value of 2,397 ppm, and their $\delta^{13}C$ values range from -3.5‰ to 3.5‰ with a weighted average value of 1.8‰ (already reported in Li et al. 2019; also see SI - Table S4). The concentrations of organic carbon in the 44-meter-thick basaltic section from DSDP Hole 543A range from 644 ppm to 3,675 ppm with a weighted average value of 1,357 ppm (SI - Table S3). The $\delta^{13}C$ values of organic carbon vary from -26.2‰ to -27.4‰ with a weighted average value of -26.6‰ (SI - Table S3). Based on these new data (Fig. 2), and previously published data on carbonate veins ($4{,}636^{\pm 464}$; Gillis & Coogan, 2011) in Hole 543A basalts, we obtained a weighted average concentration of total carbon (referred as [TC]) of the upper volcanics at Site 543 as $8{,}390^{\pm 464}$ ppm (SI - Table S3, S4 and S6). The weighted average $\delta^{13}C$ value of the upper volcanics at Site 543 is calculated as -2.8‰ by assuming that the carbonate veins have a same weighted average $\delta^{13}C$ values of 1.8‰ as the disseminated carbonate in this section. Incorporating these new data, we obtain an updated global average [TC] value of $9{,}542^{\pm 508}$ ppm (Table S6) for the upper volcanics in old (>65 Ma) AOC for further AOC carbon budget modeling (see below).

Due to the lack of samples from the lower strata (lower volcanics, transition, sheeted dike and gabbro) of the LA oceanic crust, to best estimate the [TC] values of these sections, we applied the $[TC]_{\text{Global upper volcanics}}/[TC]_{\text{LA upper volcanics}}$ ratio of 1.14 to the lower volcanics, transition, sheeted dike and gabbro to estimate the [TC] values of these lower four sections in the LA subducting slab (SI - Table S6). Applying these data, we obtained a carbon input flux of $1.16^{\pm 0.17} \times 10^{10}$ mol/yr carried by AOC into the 490 km C-N LA trench. The $\delta^{13}C$ value of the total carbon in AOC is assumed to be represented by the weighted average $\delta^{13}C$ value of -2.8‰ measured from the upper volcanics. Despite the altered oceanic crust, serpentinized uppermost mantle rocks could contribute additional carbon for subduction. However, the carbon in this reservoir is largely unknown at the C-N LA margin. They are thus not considered in the discussion below.

Combining subducting sediments and AOC together, the subducting slab has a $\delta^{13}C$ value of of ~1.9‰ for total carbonate, -25.6‰ for total organic carbon, and -2.7‰ for total carbon (SI - Text S3); the total carbon input flux into the C-N LA trench is $1.28^{\pm 0.17} \times 10^{10}$ mol/yr, in which AOC accounts for 91% of the total carbon in the C-N LA subducting slab.

3.3. Carbon Output Flux

198 The volcanic CO_2 emission data are available for the two major active volcanoes in the C-N
199 LA arc, i.e., the Soufriere Hills Volcano in Montserrat and the La Soufriere Volcano in
200 Guadeloupe. Based on the 19-year monitoring of SO_2 flux and the measured average CO_2/SO_2
201 molar ratio of the Montserrat volcanic gases (5.1±1.2; Christopher et al., 2010, 2015; Edmonds et
202 al., 2010; also see SI - Table S7), the total carbon emission flux from Montserrat was estimated to
203 be $1.57^{\pm0.37}\times10^{10}$ mol C/yr. It is noted that the large uncertainty associated with this estimate on
204 carbon emission is mostly contributed by the large variation of the CO_2/SO_2 molar ratio of the
205 Montserrat volcanic gases.
206 In a recent study, Fischer et al. (2019) used satellite-based SO_2 emission data (Carn et al.,
207 2017) to estimate the total carbon emission in Montserrat and yielded a value of 3.0×10^{10} mol
208 C/yr. The error of this value propagated from the uncertainties of SO_2 flux (Carn et al., 2017) was
209 estimated to be 58%, giving a range of 1.3-4.7×10^{10} mol/yr for the total emission. The lower end
210 of this range overlaps well with our estimate above.
211 To estimate the proportion of recycled slab carbon in the total emitted CO_2, we employed a
212 commonly used three-endmember mixing model (e.g., Sano & Marty, 1995) between the depleted
213 mantle (-5.0‰; Cartigny, 2005), slab carbonate and slab organic carbon (Supporting Information
214 Text S3). Based on the determined $\delta^{13}C$ values of slab carbonate (1.9‰) and organic carbon (-
215 25.6‰), and the presumed $CO_2/^3He$ values of these reservoirs (Sano & Williams, 1996), modeling
216 of the observed $CO_2/^3He$ and $\delta^{13}C$ data of fumarolic gases from the Montserrat volcano (Van Soest
217 et al., 1998) yielded a fraction of $81.1^{\pm1.5}$% for the recycled slab carbon in the total emitted CO_2
218 gas (see SI - Text S3, Table S8 and Fig. S3). This led to a recycled carbon output flux of $1.27^{\pm0.30}$
219 $\times10^{10}$ mol C/yr from Montserrat. It should be noted that the CO_2/SO_2 ratio of the Soufriere Hills
220 Volcano in Montserrat was obtained from gas plumes with high temperature (~720 °C) signatures
221 (Edmonds et al., 2010; Hammouya et al., 1998), which minimizes the uncertainty caused by the
222 scrubbing of magmatic sulfur by the low-temperature hydrothermal reactions (Symonds et al.,
223 2001). Crustal contamination has been brought to attention during the discussion of slab recycling
224 in the LA arc (e.g., Bezard et al., 2014, 2015; Davidson & Harmon, 1989; Van Soest et al., 2002).
225 However, the magmatic systems that were potentially affected by crustal contamination mainly lie
226 in the central to southern LA arc (Martinique to Grenada; e.g., Bezard et al., 2015; Davidson &

Harmon, 1989; Devine & Sigurdsson, 1980; Van Soest et al., 2002), whereas the northern arc, which contributes the majority of the carbon output in this study, shows minimal sign of crustal contamination based on the MORB-like helium and oxygen isotopic of olivine phenocrysts in volcanic rocks (Van Soest et al., 2002).

The CO_2 emission in the La Soufriere Volcano has been constrained by Allard et al. (2014) as $1.20^{\pm0.36} \times 10^8$ mol C/yr, which is two orders smaller than that of the Soufriere Hills Volcano in Montserrat. Applying the same three-end-member mixing model (SI - Text S3, Table S8 and Fig. S3), and the observed $CO_2/^3He$ and $\delta^{13}C$ values of fumarolic gases from the La Soufriere volcano ($-3.1^{\pm0.1}$‰; Pedroni et al., 1999; Van Soest et al., 1998), we obtained the fraction of recycled slab carbon in the total emitted CO_2 to be $88.3^{\pm2.4}$%, which led to a recycled carbon output flux of $1.06^{\pm0.32} \times 10^8$ mol C/yr from Guadeloupe.

All together, these two major volcanic systems recycle a total of $1.28^{\pm0.30} \times 10^{10}$ mol slab carbon per year. Despite the Soufriere Hills Volcano in Montserrat as a dominant emitter, the CO_2 emissions in most of the weak emitters in the C-N LA, including Dominica and Martinique, have not been instrumentally constrained yet. Brantley and Koepenick (1995) observed an exponential decrease trend in CO_2 emissions in the order of volcanic activity in a single arc chain. This suggests that the contribution of the other less active volcanoes in the C-N LA to the total carbon recycling may not be significant. Fisher et al. (2019) yielded a CO_2 emission flux of 0.3×10^{10} mol/yr (10% of the emission from Montserrat) by weak hydrothermal/magmatic emitters of the entire LA arc, which also indicates relatively small contribution from the weak emitters.

4. Discussion

4.1 Efficient Recycling of Slab Carbon at the C-N LA Arc

Previous studies investigating carbon recycling in individual subduction zones showed that the slab carbon recycled to the arc was highly variable. For example, in subduction zones which contain thick sedimentary carbonate layers, such as Izu-Bonin-Mariana and Central America (Li & Bebout, 2005; Plank & Langmuir, 1998; Sadofsky & Bebout, 2004), the amount of recycled slab carbon can be easily accounted by small fractions of carbon from subducting sediments (De Leeuw et al., 2007; Mitchell et al., 2010) and AOC. Whereas in subduction zones where the subducting sediments are carbonate-poor, such as Sunda, the recycled slab carbon cannot be easily

matched by subducting sediments and requires additional carbon from AOC to account for (House et al., 2019). However, because the carbon data in the subducting AOC have not been available until recently, the CREA values of these subduction zones have not been quantified.

Our results indicate that the C-N LA arc is similar to the Sunda case in that the recycled carbon in the arc cannot be matched by subducting sediments, but the deficit of sedimentary carbon is even larger in the C-N LA arc – the ratio of the recycled carbon output flux over the sedimentary carbon input flux in the C-N LA arc is ~11, nearly four times of that in the Sunda arc (~3; House et al., 2019). By taking into account of the AOC contributions, we yielded the CREA value of the C-N LA to be $100^{\pm 27}$%, in which the large uncertainty is mainly propagated from the uncertainty (±24%) of the CO_2/SO_2 ratio of the Montserrat volcanic gases (Edmonds et al., 2010), or >88% if employ the emission data from Fischer et al. (2019). Our new CREA value is larger than the earlier estimate (~70%) by Hilton et al. (2002) and Johnston et al. (2011). This difference may be attributed to the overestimation of carbon input flux in the earlier two studies, in which a higher carbon content and a longer effective AOC depth were applied. Nevertheless, our study is so far the first convincing case for efficient recycling of slab carbon through arc volcanism among these studied subduction zones in the world.

4.2 Minor Carbon Loss in the Forearc Region

Forearc region has been proposed by recent studies to be a potential site for significant slab carbon recycling in early subduction (e.g., Barry et al., 2019; Falk & Kelemen, 2015). Infiltration of H_2O-rich fluids to the slab in an open system behavior has been proposed to be a critical factor to enhance the decarbonation within the forearc region (e.g., Gorman et al., 2006). However, detailed petrographic and geochemical studies on metamorphosed sediments and AOC from the Italian and French Alps suggested that these subducted slabs showed closed- or limited open-system features with minimal carbon loss during forearc metamorphism (Collins et al., 2015; Cook-Kollars et al., 2014).

Along the C-N LA trench, modeling using open-system decarbonation (Gorman et al., 2006) predicted that up to ~60% of the slab carbon would be lost within the forearc region. However, the observed high CREA value of the C-N LA arc means that the majority of the slab carbon survived forearc decarbonation and was further transferred to at least the sub-arc depth. Minor carbon loss

within the forearc region indicates that the carbon cycling at the C-N LA margin does not follow the open-system decarbonation model, which is similar to the field observations in the Alps (Collins et al., 2015; Cook-Kollars et al., 2014). This implies that fluids derived from dehydration of oceanic crust may not be released via pervasive infiltration but more likely via focused channelized flow along localized structures, such as the fracture zones closely spaced from the central Martinique to northern Saba inferred from the high frequencies of small earthquakes in the C-N LA slab (Schlaphorst et al., 2016). These fracture networks facilitete rapid escape of fluid, which results in little interaction between the focused fluid and the pervasive carbon in the slab.

4.3 Substantial Carbon Release at Sub-arc Depth

Sub-arc depth is an important site for the recycling of slab carbon. The release of volatiles has been considered to be mainly controlled by the thermal structure of subducting plate (e.g., Collins et al., 2015; Gorman et al., 2006; Kerrick & Connolly, 2001a, 2001b; van Keken et al., 2011;). Thermal parameter Φ ($=A \cdot V_c \cdot \sin\theta$, in which A, V_c and θ are plate age, convergence rate and dip angle, respectively) is commonly used to describe the thermal condition of a subducting slab (e.g., Syracuse & Abers, 2006). An old slab with fast descent rate (thus a large Φ value) corresponds to a cold geotherm, whereas a young slab with slow convergence rate (thus a small Φ value) corresponds to a hot geotherm (Peacock, 2003).

Despite of a relatively old age (~87 Ma) of the C-N LA slab, the extremely slow convergence rate results in a relatively small thermal parameter (1,595±66 km), suggesting a relatively warm slab (Syracuse et al., 2010) in the LA trench. Previous modeling for closed-system decarbonation in a warm slab (e.g., Southeast Japan; Kerrick & Connolly, 2001a) still gave limited carbon loss at sub-arc depth. However, Collins et al. (2015) suggested that, if extra heat from mantle wedge is considered, far more carbon release would occur at sub-arc depth. Our observation from the C-N LA arc clearly shows substantial carbon release at the sub-arc depth of a relatively warm slab (**Fig. 3**). This in turn implies that previous modeling studies (e.g., Kerrick & Connolly, 2001a, 2001b) might have underestimated the thermal structure of some subduction zones. This conclusion is also consistent with recent studies (e.g., Penniston-Dorland et al., 2015) showing that the thermal structure of subduction zones recorded by exhumed high-pressure rocks is warmer than that predicted by models (e.g., Gerya et al., 2002; Syracuse et al., 2010).

4.4 Implications to Global Carbon Recycling

Our new data demonstrate that, in the C-N LA subduction zone, the slab carbon has been well preserved throughout the forearc region but substantially released at the sub-arc depth. The observed minimal slab carbon loss in the forearc region is different to recent field studies in Central America suggesting that significant slab carbon is remobilized from the slab to the forearc region (e.g., Barry et al., 2019). The observed efficient recycling of slab carbon at the sub-arc depth is also inconsistent with thermodynamic and experimental predictions that common carbon-bearing minerals in subducting slabs are stable well beyond the sub-arc depth (e.g., Kerrick & Connolly, 2001a, 2001b; Molina & Poli, 2000). These observations from the C-N LA case highlight the strong variability and complexity in carbon recycling through arc on a global scale. The carbon behavior in a slab is likely controlled by multiple factors (e.g., Collins et al., 2015; Gorce et al., 2019; Gorman et al., 2006; Johnston et al., 2011; Kerrick & Connolly, 2001a, 2001b), among which some (e.g., slab age, subducting rate) may show a general pattern and their effects can be modelled on a global scale, whereas others (e.g., carbonate enrichment in subducting sediments and AOC, water flux, fracture network, oxygen fugacity) may change significantly among different subduction zones (e.g., Jarrard, 2003; Plank & Langmuir, 1998). These site-specific features may strongly affect the carbon behavior (e.g., open- or closed system; carbon loss or preservation) in individual slab, but may not be included in a simple box model. These heterogeneities are needed to be fully considered in future study of global carbon recycling.

5. Conclusions

Carbon input flux into the Central-Northern Lesser Antilles trench is estimated to be 1.21×10^{9} mol/yr for subducting sediments and $1.16^{\pm0.17}\times10^{10}$ mol/yr for altered oceanic crust, based on measurements of organic carbon and carbonate in both reservoirs. Recycled slab carbon output flux via the C-N LA volcanoes is estimated to be $1.28^{\pm0.30}\times10^{10}$ mol C/yr, based on modeling of previously published volcanic emission data. The identical numbers between the input and output carbon fluxes indicate efficient recycling of the slab carbon through the C-N LA arc. This indicates little loss of slab carbon in the fore-arc region of the C-N LA subduction zone. Integrated with published results from other subduction zones, our new observations highlight

strongly variable carbon behavior in global subduction zones and emphasizes that the understanding of subduction-zone carbon cycle should be built on integrated results of individual subduction zones in which carbon recycling may be dominated by different physiochemical properties.

Acknowledgement

This study was supported by NSERC Discovery grant to LL. This research used samples provided by the Deep Sea Drilling Program (DSDP). We thank Dr. Edmonds for providing the SO_2 flux data of Montserrat to facilitate our modeling. The manuscript benefited from constructive comments from two anonymous reviewers.

Data supporting this study are available at https://data.mendeley.com/drafts/7n6n4vh2yg.

Figure captions

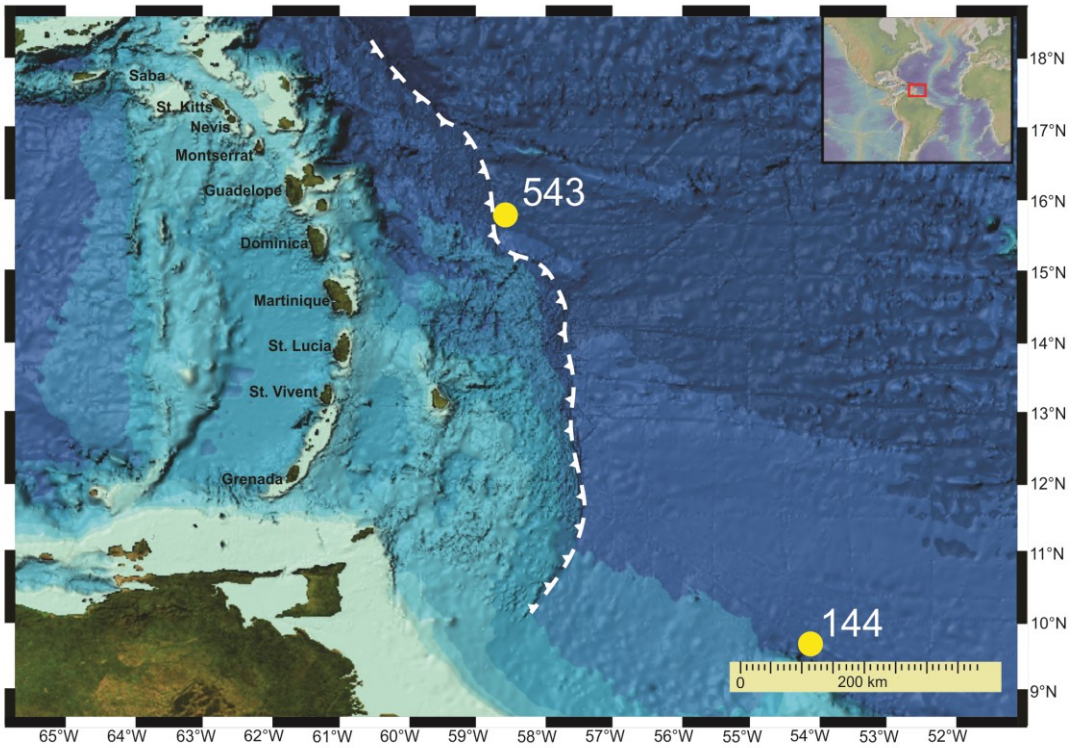

Fig. 1 Lesser Antilles volcanic arc and the associated Deep See Drilling Cores (DSDP Site 543 and Site 144) (the map is generated by the GeoMapApp: http://www.geomapapp.org). The white dashed line represents the trench where the slow spreading slab is subducting. The C-N Lesser Antilles stretches from Martinique island in the central part to the Saba island in the Northern part.

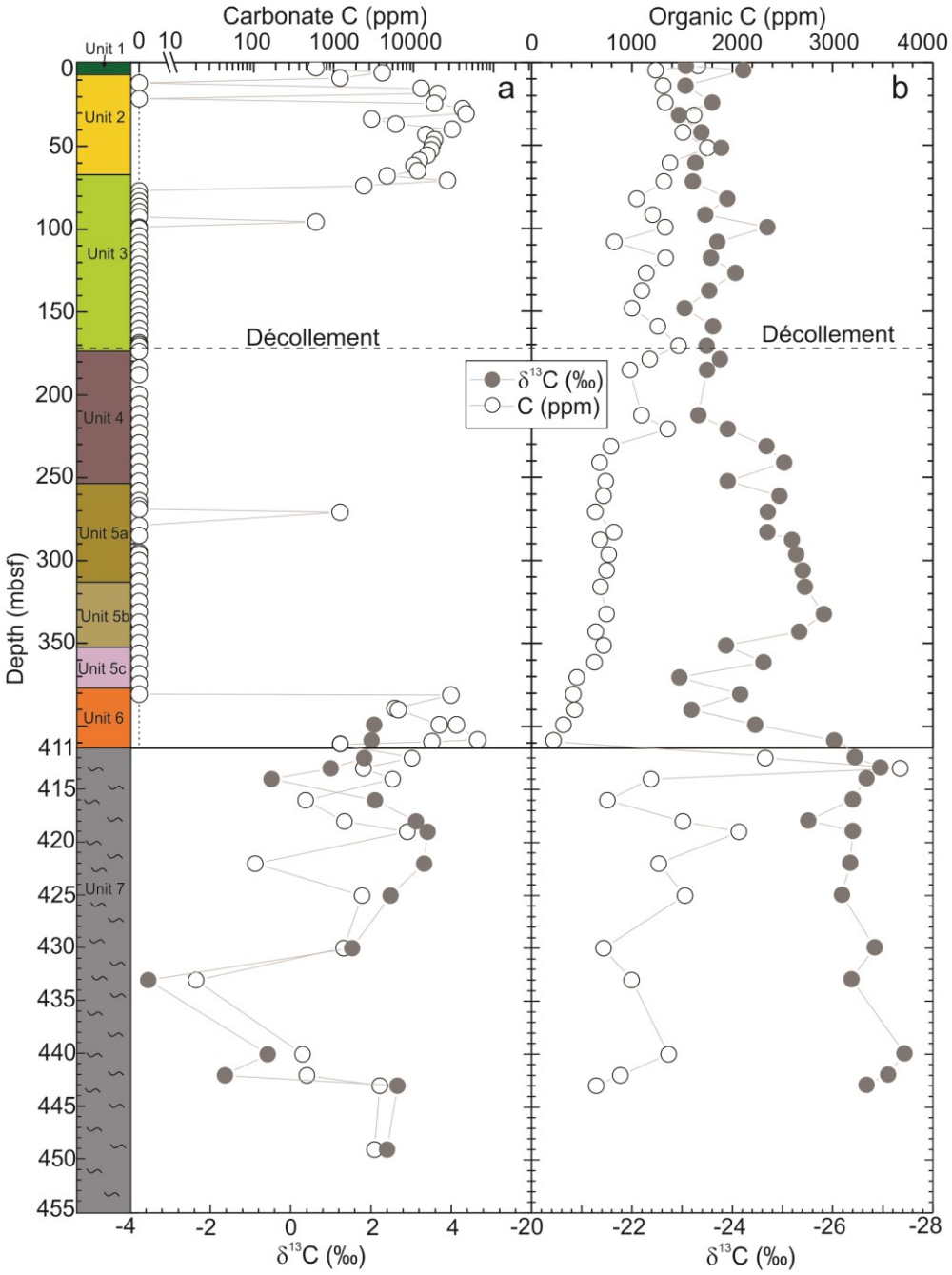

Fig. 2 Carbon concentration and isotopic composition of Site 543. Site 543 is divided into 7 units based on the lithology – Unit 1: 8-m-thick Quaternary ashy mud; Unit 2: 60-m-thick lower Pleistocene to upper Pliocene ashy nannofossil mud with ash layers; Unit 3: 105-m-thick lower Pliocene to Miocene mud; Unit 4: 79-m-thick lower Miocene to Oligocene radiolarian clay with ashy layers; Unit 5a: 60-m-thick Oligocene to middle late Eocene radiolarian clay; Unit 5b: 38-m-thick Eocene zeolitic claystone; Unit 5c: 28-m-thick Eocene claystone; Unit 6: 32-m-thick late Maastrichtian to lower Campanian calcareous ferruginous claystone; Unit 7: 44-m-thcik pillow basalt (Shipboard Scientific Party, 1984). The horizontal dashed line is the décollement at ~171 m below the seafloor. (a) Carbonate carbon concentration and $\delta^{13}C$ values of Site 543 sediments and AOC (grey circle: $\delta^{13}C$ values; empty circle: carbon concentration). Carbonate carbon concentration data is from Wright. (1984). (b) Organic carbon concentration and $\delta^{13}C$ values of Site 543 sediments and AOC.

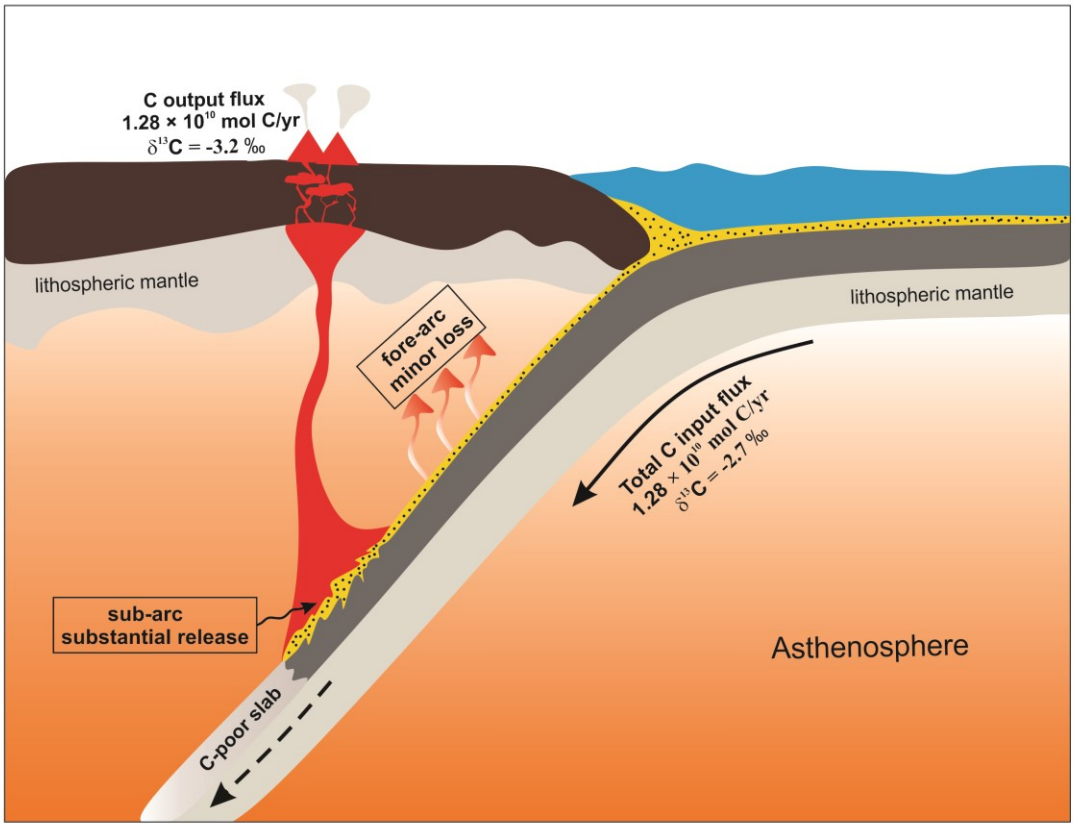

Fig. 3 Schematic diagram showing the carbon recycling model at C-N Lesser Antilles Arc. The total carbon input flux contributed by sediments and altered oceanic crust is ~1.28 x 10^{10} mol/yr, which is identical to the flux of recycled carbon of ~1.28 x 10^{10} mol/yr through the C-N LA arc volcanoes. This suggests minimal carbon loss within the forearc region and subduction of carbon-poor slab into the deep mantle in this region.

References

Ague, J.J., & Nicolescu, S. (2014) Carbon dioxide released from subduction zones by fluid-mediated reactions. *Nature Geoscience*, 7(5), 355-360. https://doi.org/10.1038/ngeo2143

Allard, P., Aiuppa, A., Beauducel, F., Gaudin, D., Di Napoli, R., Calabrese, S., et al. (2014) Steam and gas emission rate from La Soufriere volcano, Guadeloupe (Lesser Antilles): implications for the magmatic supply during degassing unrest. *Chemical Geology*, 384, 76-93. https://doi.org/10.1016/j.chemgeo.2014.06.019

Alt, J.C., & Teagle, D.A.H. (1999) The uptake of carbon during alteration of ocean crust. *Geochimica et Cosmochimica Acta*, 63, 1527-1535. https://doi.org/10.1016/S0016-7037(99)00123-4

Barry, P., de Moor, J., Giovannelli, D., Schrenk, M., Hummer, D., Lopez, T., Pratt, C., et al. (2019) Forearc carbon sink reduces long-term volatile recycling into the mantle. *Nature*, 568(7753), 487-492. https://doi.org/10.1038/s41586-019-1131-5

Behn, M.D., Kelemen, P.B., Hirth, G., Hacker, B.R., & Massonne, H.-J. (2011) Diapirs as the source of the sediment signature in arc lavas. *Nature Geoscience*, 4(9), 641-646. https://doi.org/10.1038/ngeo1214

Bezard, R., Davidson, J.P., Turner, S., Macpherson, C.G., Lindsay, J.M., & Boyce, A.J. (2014) Assimilation of sediments embedded in the oceanic arc crust: myth or reality? *Earth and Planetary Sciecne Letters*, 395, 51-60. https://doi.org/10.1016/j.epsl.2014.03.038

Bezard, R., Schaefer, B.F., Turner, S., Davidson, J.P., & Selby, D. (2015) Lower crustal assimilation in oceanic arcs: Insights from an osmium isotopic study of the Lesser Antilles. *Geochimica et Cosmochimica Acta*, 150, 330-344. https://doi.org/10.1016/j.gca.2014.11.009

Bouysse, P., Westercamp, D., & Andereiredd, P. (1990) The Lesser Antilles Island Arc, in: In Moore, J.C., Mascle, A., et al. (Eds.) *Proceedings of the Ocean Drilling Program, Scientific. Results*, Ocean Drilling Program, College Station, TX, pp. 29-44. http://doi:10.2973/odp.proc.sr.110.166.1990

Brantley, S.L., & Koepenick, K.W. (1995) Measured carbon dioxide emissions from Oldoinyo Lengai and the skewed distribution of passive volcanic fluxes. *Geology*, 23(10), 933-936. https://doi.org/10.1130/0091-7613(1995)023

Carn, S., Fioletov, V., McLinden, C., Li, C., & Krotkov, N. (2017) A decade of global volcanic SO 2 emissions measured from space. *Scientific reports*, 7, 44095. https://doi.org/10.1038/srep44095

Carpentier, M., Chauvel, C., & Mattielli, N. (2008) Pb–Nd isotopic constraints on sedimentary input into the Lesser Antilles arc system. *Earth and Planetary Sciecne Letters*, 272, 199-211. https://doi.org/10.1016/j.epsl.2008.04.036

Cartigny, P. (2005) Stable isotopes and the origin of diamond. *Elements* 1(2), 79-84. https://doi.org/10.2113/gselements.1.2.79

Christopher, T., Blundy, J., Cashman, K., Cole, P., Edmonds, M., Smith, P., et al. (2015) Crustal-scale degassing due to magma system destabilization and magma-gas decoupling at Soufrière Hills Volcano, Montserrat. *Geochemistry, Geophysics. Geosystystems*, 16(9), 2797-2811. https://doi.org/10.1002/2015GC005791

Christopher, T., Edmonds, M., Humphreys, M.C., & Herd, R.A. (2010) Volcanic gas emissions from Soufrière Hills Volcano, Montserrat 1995–2009, with implications for mafic magma supply and degassing. *Geophysical Research Letters*, 37(19). https://doi.org/10.1029/2009GL041325

Collins, N.C., Bebout, G.E., Angiboust, S., Agard, P., Scambelluri, M., Crispini, L., & John, T. (2015) Subduction zone metamorphic pathway for deep carbon cycling: II. Evidence from HP/UHP

metabasaltic rocks and ophicarbonates. *Chemical Geology*, 412, 132-150. https://doi.org/10.1016/j.chemgeo.2015.06.012

Cook-Kollars, J., Bebout, G.E., Collins, N.C., Angiboust, S., & Agard, P. (2014) Subduction zone metamorphic pathway for deep carbon cycling: I. Evidence from HP/UHP metasedimentary rocks, Italian Alps. *Chemical Geology*, 386, 31-48. https://doi.org/10.1016/j.chemgeo.2014.07.013

Davidson, J.P., & Harmon, R.S. (1989) Oxygen isotope constraints on the petrogenesis of volcanic arc magmas from Martinique, Lesser Antilles. *Earth and Planetary Science Letters*, 95, 255-270. https://doi.org/10.1016/0012-821X(89)90101-5

De Leeuw, G., Hilton, D., Fischer, T., & Walker, J. (2007) The He–CO2 isotope and relative abundance characteristics of geothermal fluids in el salvador and honduras: New constraints on volatile mass balance of the central american volcanic arc. *Earth and Planetary Science Letters*, 258, 132-146. https://doi.org/10.1016/j.epsl.2007.03.028

Devine, J., & Sigurdsson, H. (1980) Garnet–fassaite calc-silicate nodule from La Soufrière, St. Vincent. *American Mineralogist*, 65(3-4), 302-305.

Edmonds, M., Aiuppa, A., Humphreys, M., Moretti, R., Giudice, G., Martin, R., et al. (2010) Excess volatiles supplied by mingling of mafic magma at an andesite arc volcano. *Geochemistry, Geophysics. Geosystystems*, 11(4), Q04005. https://doi.org/10.1029/2009GC002781

Falk, E.S., & Kelemen, P.B. (2015) Geochemistry and petrology of listvenite in the Samail ophiolite, Sultanate of Oman: Complete carbonation of peridotite during ophiolite emplacement. *Geochimica et Cosmochimica Acta*, 160, 70-90. https://doi.org/10.1016/j.gca.2015.03.014

Fischer, T.P., Arellano, S., Carn, S., Aiuppa, A., Galle, B., Allard, P., et al. (2019) The emissions of CO_2 and other volatiles from the world's subaerial volcanoes. *Scientific Reports*, 9(1), 1-11. https://doi.org/10.1038/s41598-019-54682-1

Frezzotti, M.L., Selverstone, J., Sharp, Z.D., & Compagnoni, R. (2011) Carbonate dissolution during subduction revealed by diamond-bearing rocks from the Alps. *Nature Geoscience*, 4(10), 703-706. https://doi.org/10.1038/ngeo1246

Galvez, M., Beyssac, O., Martinez, I., & Malavieille, J. (2013) Graphite formation by carbonate reduction during subduction. *Nature Geoscience*, 6(6), 473-477. https://doi.org/10.1038/ngeo1827

Germa, A., Quidelleur, X., Labanieh, S., Chauvel, C., & Lahitte, P. (2011) The volcanic evolution of Martinique Island: Insights from K–Ar dating into the Lesser Antilles arc migration since the Oligocene. *Journal of Volcanology and Geothermal Research*, 208(3-4), 122-135. https://doi.org/10.1016/j.jvolgeores.2011.09.007

Gerya, T.V., Stöckhert, B., & Perchuk, A.L. (2002) Exhumation of high-pressure metamorphic rocks in a subduction channel: A numerical simulation. *Tectonics*, 21(6), 6-1. https://doi.org/10.1029/2002TC001406

Gillis, K., & Coogan, L. (2011) Secular variation in carbon uptake into the ocean crust. *Earth and Planetary Science Letters*, 302, 385-392. https://doi.org/10.1016/j.epsl.2010.12.030

Gorce, J., Caddick, M., & Bodnar, R. (2019) Thermodynamic constraints on carbonate stability and carbon volatility during subduction. *Earth and Planetary Science Letters*, 519, 213-222. https://doi.org/10.1016/j.epsl.2019.04.047

Gorman, P.J., Kerrick, D., & Connolly, J. (2006) Modeling open system metamorphic decarbonation of subducting slabs. *Geochemistry, Geophysics. Geosystystems*, 7(4), Q04007. https://doi.org/10.1029/2005GC001125

Hammouya, G., Allard, P., Jean-Baptiste, P., Parello, F., Semet, M., & Young, S. (1998) Pre-and syn-

eruptive geochemistry of volcanic gases from Soufriere Hills of Montserrat, West Indies. *Geophysical Research Letters*, 25(19), 3685-3688. https://doi.org/10.1029/98GL02321

Hilton, D.R., Fischer, T.P., & Marty, B. (2002) Noble gases and volatile recycling at subduction zones. *Reviews in Mineralogy and Geochemistry*, 47(1), 319-370. https://doi.org/10.2138/rmg.2002.47.9

House, B.M., Bebout, G.E., & Hilton, D.R. (2019) Carbon cycling at the Sunda margin, Indonesia: A regional study with global implications. *Geology*, 47(5), 483-486. https://doi.org/10.1130/G45830.1

Jarrard, R.D. (2003) Subduction fluxes of water, carbon dioxide, chlorine, and potassium. *Geochemistry, Geophysics. Geosystystems*, 4(5), 1-21. https://doi.org/10.1029/2002GC000392

Johnston, F.K., Turchyn, A.V., & Edmonds, M. (2011) Decarbonation efficiency in subduction zones: Implications for warm Cretaceous climates. *Earth and Planetary Science Letters*, 303, 143-152. https://doi.org/10.1016/j.epsl.2010.12.049

Kelemen, P.B., & Manning, C.E. (2015) Reevaluating carbon fluxes in subduction zones, what goes down, mostly comes up. *Proceedings of the National Academy of Sciences. Natl. U.S.A,* 112, E3997-E4006. https://doi.org/10.1073/pnas.1507889112

Kerrick, D.M., & Connolly, J.A.D. (2001a) Metamorphic devolatilization of subducted oceanic metabasalts: implications for seismicity, arc magmatism and volatile recycling. *Earth and Planetary Science Letters*, 189, 19-29. https://doi.org/10.1016/S0012-821X(01)00347-8

Kerrick, D.M., & Connolly, J.A.D. (2001b) Metamorphic devolatilization of subductedmarine sediments and the transport of volatiles into the Earth's mantle. *Nature*, 411(6835), 293-296. https://doi.org/10.1038/35077056

Labanieh, S., Chauvel, C., Germa, A., Quidelleur, X., & Lewin, E. (2010) Isotopic hyperbolas constrain sources and processes under the Lesser Antilles arc. *Earth and Planetary Science Letters*, 298, 35-46. https://doi.org/10.1016/j.epsl.2010.07.018

Li, K., Li, L., Pearson, D.G., & Stachel, T. (2019) Diamond isotope compositions indicate altered igneous oceanic crust dominates deep carbon recycling. *Earth and Planetary Science Letters*, 516, 190-201. https://doi.org/10.1016/j.epsl.2019.03.041

Li, L., & Bebout, G.E. (2005) Carbon and nitrogen geochemistry of sediments in the Central American convergent margin: insights regarding subduction input fluxes, diagenesis, and paleoproductivity. *Journal of Geophysical Research: Solid Earth*, 110(B11). https://doi.org/10.1029/2004JB003276

Marschall, H.R., & Schumacher, J.C. (2012) Arc magmas sourced from mélange diapirs in subduction zones. *Nature Geoscience*, 5(12), 862-867. https://doi.org/10.1038/ngeo1634

Martin, L. A., & Hermann, J. (2018). Experimental phase relations in altered oceanic crust: implications for carbon recycling at subduction zones. Journal of Petrology, 59, 299–320. https://doi.org/10.1093/petrology/egy031

Mitchell, E.C., Fischer, T.P., Hilton, D.R., Hauri, E.H., Shaw, A.M., de Moor, J.M.,et al. (2010) Nitrogen sources and recycling at subduction zones: Insights from the Izu-Bonin-Mariana arc. *Geochemistry, Geophysics. Geosystystems*, 11(2), Q02X11. https://doi.org/10.1029/2009GC002783

Molina, J.F., & Poli, S. (2000) Carbonate stability and fluid composition in subducted oceanic crust: an experimental study on H2O–CO2-bearing basalts. *Earth and Planetary Science Letters*, 176, 295-310. https://doi.org/10.1016/S0012-821X(00)00021-2

Peacock, S.M. (2003) Thermal structure and metamorphic evolution of subducting slabs. *Geophysical Monograph-American Geophysical Union* 138, 7-22. https://doi.org/10.1029/138GM02

Pedroni, A., Hammerschmidt, K., & Friedrichsen, H. (1999) He, Ne, Ar, and C isotope systematics of geothermal emanations in the Lesser Antilles Islands Arc. *Geochimica et Cosmochimica Acta*, 63,

515-532. https://doi.org/10.1016/S0016-7037(99)00018-6

Penniston-Dorland, S.C., Kohn, M.J., & Manning, C.E. (2015) The global range of subduction zone thermal structures from exhumed blueschists and eclogites: Rocks are hotter than models. *Earth and Planetary Science Letters*, 428, 243-254. https://doi.org/10.1016/j.epsl.2015.07.031

Piccoli, F., Brovarone, A.V., Beyssac, O., Martinez, I., Ague, J.J., & Chaduteau, C. (2016) Carbonation by fluid–rock interactions at high-pressure conditions: Implications for carbon cycling in subduction zones. *Earth and Planetary Science Letters*, 445, 146-159. https://doi.org/10.1016/j.epsl.2016.03.045

Plank, T., Kelley, K.A., Murray, R.W., & Stern, L.Q. (2007) Chemical composition of sediments subducting at the Izu-Bonin trench. *Geochemistry, Geophysics. Geosystystems*, 8(4), Q04116. https://doi.org/10.1029/2006GC001444

Plank, T., & Langmuir, C.H. (1998) The chemical composition of subducting sediment and its consequences for the crust and mantle. *Chemical Geology*, 145, 325-394. https://doi.org/10.1016/S0009-2541(97)00150-2

Sadofsky, S.J., & Bebout, G.E. (2004) Nitrogen geochemistry of subducting sediments: New results from the Izu-Bonin-Mariana margin and insights regarding global nitrogen subduction. *Geochemistry, Geophysics. Geosystystems*, 5(3), Q03115. https://doi.org/10.1029/2003GC000543

Sano, Y., & Marty, B. (1995) Origin of carbon in fumarolic gas from island arcs. *Chemical Geology*, 119, 265-274. https://doi.org/10.1016/0009-2541(94)00097-R

Sano, Y., & Williams, S.N. (1996) Fluxes of mantle and subducted carbon along convergent plate boundaries. *Geophysical Research Letters*, 23(20), 2749-2752. https://doi.org/10.1029/96GL02260

Scambelluri, M., Bebout, G.E., Belmonte, D., Gilio, M., Campomenosi, N., Collins, N., & Crispini, L. (2016) Carbonation of subduction-zone serpentinite (high-pressure ophicarbonate; Ligurian Western Alps) and implications for the deep carbon cycling. *Earth and Planetary Science Letters*, 441, 155-166. https://doi.org/10.1016/j.epsl.2016.02.034

Schlaphorst, D., Kendall, J.-M., Collier, J.S., Verdon, J.P., Blundy, J., Baptie, B., et al. (2016) Water, oceanic fracture zones and the lubrication of subducting plate boundaries—insights from seismicity. *Geophysical Journal International*, 204(3), 1405-1420. https://doi.org/10.1093/gji/ggv509

Shaw, A.M., Hilton, D.R., Fischer, T.P., Walker, J.A., & Alvarado, G.E. (2003) Contrasting He–C relationships in Nicaragua and Costa Rica: insights into C cycling through subduction zones. *Earth and Planetary Science Letters*, 214, 499-513. https://doi.org/10.1016/S0012-821X(03)00401-1

Shipboard scientific Party (1972) Sites 143 and 144, in: Hayes, D.E., Pimm, A.C., Beckmann, J.P., W Benson, i.E., Berger, W.H., Roth, P.H., Supko, P.R., Rad, U.v. (Eds.) *Initial Reports of Deep Sea Drilling Program*, U.S. Government Printing Office, Washington, pp. 284-338. http://doi:10.2973/dsdp.proc.14.110.1972

Shipboard Scientific Party (1984) Site 543: Oceanic Referenc Site East of the Barbados Ridge Complex, in: Biju-Duval, B., Moore, J. A.M., Blackinton, G., Claypool, G.E., Cowan, D.S., (Eds.) *Initial Reports of Deep Sea Drilling Program*, U.S. Govt. Printing Office, Washington, pp. 227-298. http://doi:10.2973/dsdp.proc.78a.110.1984

Stein, C.A., & Stein, S. (1992) A model for the global variation in oceanic depth and heat flow with lithospheric age. *Nature*, 359(6391), 123-129. https://doi.org/10.1038/359123a0

Symonds, R., Gerlach, T., & Reed, M. (2001) Magmatic gas scrubbing: implications for volcano monitoring. *Journal of Volcanology and Geothermal Research* 108, 303-341. https://doi.org/10.1016/S0377-0273(00)00292-4

Syracuse, E.M., & Abers, G.A. (2006) Global compilation of variations in slab depth beneath arc volcanoes and implications. *Geochemistry, Geophysics. Geosystystems*, 7(5), Q05017. https://doi.org/10.1029/2005GC001045

Syracuse, E.M., van Keken, P.E., & Abers, G.A. (2010) The global range of subduction zone thermal models. *Physics of the Earth and Planetary Interiors*, 183(1-2), 73-90. https://doi.org/10.1016/j.pepi.2010.02.004

van Keken, P.E., Hacker, B.R., Syracuse, E.M., & Abers, G.A. (2011) Subduction factory: 4. Depth-dependent flux of H2O from subducting slabs worldwide. *Journal of Geophysical Research Letter: Solid Earth*, 116(B1). https://doi.org/10.1029/2010JB007922

Van Soest, M., Hilton, D., & Kreulen, R. (1998) Tracing crustal and slab contributions to arc magmatism in the Lesser Antilles island arc using helium and carbon relationships in geothermal fluids. *Geochimica et Cosmochimica Acta*, 62, 3323-3335. https://doi.org/10.1016/S0016-7037(98)00241-5

Van Soest, M.C., Hilton, D.R., MacPherson, C.G., & Mattey, D.P. (2002) Resolving sediment subduction and crustal contamination in the Lesser Antilles Island Arc: a combined He–O–Sr isotope approach. *Journal of Petrology* 43, 143-170. https://doi.org/10.1093/petrology/43.1.143

Wright., A. (1984) Sediment Accumulation Rates of the Lesser Antilles Intraoceanic Island Arc, Deep Sea Drilling Project Leg 78A, in: Biju-Duval, B., Moore, J. A.M., Blackinton, G., Claypool, G.E., Cowan, D.S., (Eds.) *Initial Reports of Deep Sea Drilling Program*, U.S. Govt. Printing Office, Washington, pp. 357-368. http://doi:10.2973/dsdp.proc.78a.114.1984

Supporting Information for

Efficient Carbon Recycling at the Central-Northern Lesser Antilles Arc: Implications to deep carbon recycling in global subduction zones

Authors: Kan Li[1,*], Long Li[1], Cyril Aubaud[2], Karlis Muehlenbachs[1]

Affiliations:

[1]Department of Earth and Atmospheric Sciences, University of Alberta, Edmonton, Alberta, Canada.

[2]Laboratoire de Geochimie des Isotopes Stables, Institut de Physique du Globe, Université de Paris, France

Contents of this file

Introduction

This Supporting Information provides 3 supplementary texts, 7 supplementary tables and 2 supplementary figures to support the discussion in the main article.

Text S1 is the analytical method for the analyses of organic and inorganic carbon contents in seafloor sediments and altered oceanic crust.

Text S2 describes the method for the calculation of the isotherm depth of 100 ºC within altered oceanic crust.

Text S3 describes in detail the three-end-member mixing model to determine the fraction of recycled slab carbon.

Table S1 and S2 list the contents and isotopic compositions of carbonate and organic carbon in sediments from DSDP Hole 543.

Table S3 and S4 lists the contents and isotopic compositions of carbonate and organic carbon in altered oceanic crust from DSDP Hole 543A.

Table S5 lists the contents and isotopic compositions of carbonate and organic carbon in sediments from DSDP Site 144.

Table S6 summarizes the global average content of total carbon ([TC]) of different layers (upper volcanics, lower volcanics, transition, sheeted dike and gabbro) in old AOC (>65 Ma) and the determined [TC] values of lower volcanics, transition, sheeted dike and gabbro in the 87 Ma old AOC being subducting along the Central-Northern Lesser Antilles trench.

Table S7 lists the summarized SO_2 and CO_2 fluxes of the major active volcanoes (i.e., Montserrat and Guadeloupe) in the Central-Northern Lesser Antilles.

Table S8 lists the volcanic gas data from Montserrat and Guadeloupe that were used in the three end-member mixing model.

Fig. S1 shows the along-depth variations in contents and isotopic compositions of carbonate

and organic carbon in sediments from DSDP Site 144.

Fig. S2 shows the 19-year (1996-2014) cumulative SO_2 flux at the the Soufriere Hills Volcano, Montserrat, which gives an average SO_2 flux of 0.1971 Mt/year.

Fig. S3 shows the three end-member mixing model based on the volcanic gas data.

Text S1. Analytical Methods

S1.1 Sediments:

Carbonate: Bulk sediment samples were loaded into glass vials with a septum caps, which were then installed on an autosampler tray. Following the removal of air in the glass vials by flushing with ultrahigh-purity helium gas, 100% H_3PO_4 was added each vial to react with the carbonate in the sample to release CO_2, which was then carried by an ultrahigh-purity helium stream for carbon and oxygen isotope measurements on an GV Instruments Analytical Precision AP2003 isotope ratio mass spectrometer equipped with an automated Gilson 22X autosampler at the Institut de Physique du Globe de Paris. This continuous flow system is equipped with a Nafion membrane for water removal and a gas chromatograph (GC) column (see detailed description in Assayag et al., 2006). The isotope compositions are reported in the δ notation. Analytical uncertainty (2σ) based on repeated analyses of NBS18 is better than 0.2‰ for both $\delta^{13}C$ and $\delta^{18}O$.

Organic carbon: decalcified samples were loaded to pre-cleaned quartz tubes, together with Cu_xO_x reagent. The tubes were then installed into a glass manifold to pump to high vacuum, and subsequently sealed under vacuum. The sealed tubes were first put into a muffle furnace to combust overnight at 900 ºC to oxidize organic matter into CO_2, and then cracked in the same glass manifold to extract, purify and quantify the produced CO_2, which was finally collected into a sample tube for carbon isotope measurements in a Thermo Delta V isotope-ratio mass spectrometer at dual-inlet mode. Analytical uncertainty (2σ) based on repeated analyses of USGS 24 is better than 0.15‰ for both $\delta^{13}C$.

S1.2 Altered Oceanic Crust:

Carbonate: carbon contents and isotope compositions of carbonate in 14 basaltic samples have been reported with a detailed method description by Li et al. (2019).

Organic carbon: decalcified sample powders were wrapped in pre-cleaned copper foil together with Cu_xO_x reagent and a ~3cm silver wire were loaded into quartz tubes. After over-night pumping, the tubes were sealed under high vacuum and combusted at 900 ºC overnight in a muffle furnace.

The produced CO_2 was then released by cracking the tube. After cryogenically purification and quantification, the CO_2 was collected in a sample tube and sent to a Thermo Finnigan MAT 252 isotope-ratio mass spectrometer for isotope measurements at dual-inlet mode at the University of Alberta. Analytical uncertainty (2σ) based on repeated analyses of USGS 24 is better than 0.15‰ for both $\delta^{13}C$.

Text S2. Determining the 100 ºC isotherm Depth

The estimation of the 100 ºC isotherm depth in the oceanic crust outboard the Central-Northern Lesser Antilles trench requires a few parameters, such as heat flow, sediment thickness overlying the oceanic crust, thermal conductivity of oceanic crust and sediments. The heat flow of the oceanic crust entering the Central-Northern Lesser Antilles trench is acquired by Simple Plate Cooling model (Stein & Stein, 1992). The yielded heat flow of 56±6 Mw/m^2 for the ~87 Ma oceanic crust is consistent with the instrumental data measured at Site 543 (Davis & Hussong., 1984). The sediment thickness at Site 543 is 411 m (Shipboard Scientific Party, 1984). Thermal conductivity of sediment and oceanic crust is given by Johnson and Pruis (2003). Based on these data, we modelled the temperature profile from the seawater-sediment interface, where temperature is set as 0 ºC, into the oceanic crust. The results indicate that the 100 ºC isotherm is located at 3079^{+342}_{-280} meters below the sediment-basement interface for the 87 Ma oceanic crust that is subducting into the Central-Northern Lesser Antilles trench (See Li et al., 2019 for detailed method).

Text S3. Three End-member Mixing

To determine the relative contributions of the depleted-mantle (M)-, slab carbonate (CAR)-, and slab organic carbon (ORG)- to CO_2 released in the arc (e.g., fumarolic gases and geothermal fluids), we follow the equations developed by Sano and Marty (1995) and Sano and Williams (1996):

$$\delta^{13}C_o = M \cdot \delta^{13}C_M + CAR \cdot \delta^{13}C_{CAR} + ORG \cdot \delta^{13}C_{ORG} \quad (1)$$

$$1/\left(\frac{^{12}C}{^{3}He}\right)_o = M/\left(\frac{^{12}C}{^{3}He}\right)_M + CAR/\left(\frac{^{12}C}{^{3}He}\right)_{CAR} + ORG/\left(\frac{^{12}C}{^{3}He}\right)_{ORG} \quad (2)$$

$$\mathrm{M} + \mathrm{ORG} + \mathrm{CAR} = 1 \quad (3)$$

In which O, M, CAR and ORG represent the observed value, the depleted mantle, slab carbonate, and slab organic carbon, respectively. Slab carbonate and organic carbon include these in both subducting sediments and altered oceanic crust. Although the $\delta^{13}C$ values of carbonate and organic

carbon in the entire AOC section have not been constrained due to the lack of samples from the lower oceanic crustal sections, given that ~80% of carbonate and organic carbon (both produced by low-temperature alteration; Li et al., 2019) in AOC is stored in the upper 600 meters volcanic sections, the $\delta^{13}C$ values of carbonate and organic carbon may be represented by the r $\delta^{13}C$ values of upper 44-meters basaltic samples. Accordingly, the weighted average $\delta^{13}C$ values of carbonate (1.8‰) and organic carbon (-26.6‰) measured from the upper 44-meters volcanic section (Fig. 2) are thus used to integrate with the weighted average $\delta^{13}C$ values of carbonate (2.0‰) and organic carbon (-24.5‰) of sediments (Fig. 2), to yield average values of ~-25.6‰ and ~1.9‰ for the organic and carbonate carbon, respectively, in the entire slab.

In the three-end-member mixing, $\delta^{13}C_M$, $\delta^{13}C_{ORG}$ and $\delta^{13}C_{CAR}$ values are -5.0‰, ~-25.6‰ and ~1.9‰, respectively. The helium isotopes ($^3He/^4He$) are low ($^3He/^4He$ ~ 0.05 R_A; R_A is the atmospheric $^3He/^4He$ ratio = 1.4×10^{-6}) for the slab and relatively high (8±1 R_A) for the mantle (Allègre et al., 1995). Given that the low $^3He/^4He$ values can be a result of significant crustal contamination, only volcanic gas samples with of air-corrected $^3He/^4He$ values higher than the average arc value (5.4 ± 1.9 R_A; Hilton et al., 2002) are considered not to be contaminated significantly by continental crust and thus used in the modeling here. Taking the values of $(^{12}C/^3He)_M$ = 1.5×10^9, $(^{12}C/^3He)_S$ = 10^{13}, $(^{12}C/^3He)_L$ = 10^{13} (Sano and Marty, 1995; Sano and Williams, 1996), together with the observed $CO_2/^3He$ and $\delta^{13}C$ values of fumarolic gases (Supporting information Table S8), the percentage of carbon provided by the three components M, CAR, and ORG can be quantitatively calculated based on the three end-member mixing model (Supporting information Table S8 and Fig. S3).

Table S1 Carbonate carbon contents of DSDP Hole 543 and 543A sediments below the décollement

Location	Leg-Site	Sample Number	Depth (mbsf)	Bulk Carbonate C (ppm)[a]	Carbonate C $\delta^{13}C$ (‰)[b]	Ref
Atlantic	78-543	1R-2 56-59	2	600	0.2	Wright., 1984
Atlantic	78-543	1R-3 55-56	6.2	4080	\	Wright, 1984
Atlantic	78-543	1R-4 111-118	9.3	1200	\	Wright, 1984
Atlantic	78-543	1R-7 90-93	12.4	0	\	Wright, 1984
Atlantic	78-543	2R-3 44-47	15.5	12480	1.3	Wright, 1984
Atlantic	78-543	2R-3 58-59	18.6	20160	\	Wright, 1984
Atlantic	78-543	2R-5 44-47	21.7	0	\	Wright, 1984
Atlantic	78-543	3R-3 120-123	24.8	18360	1.3	Wright, 1984
Atlantic	78-543	3R-5 40-43	27.9	41040	\	Wright, 1984
Atlantic	78-543	3R-5 56-57	31	45120	\	Wright, 1984
Atlantic	78-543	4R-2 60-63	34.1	3000	\	Wright, 1984
Atlantic	78-543	4R-2 89-90	37.2	6000	\	Wright, 1984
Atlantic	78-543	4R-4 60-63	40.3	30480	\	Wright, 1984
Atlantic	78-543	4R-6 130-133	43.4	14280	\	Wright, 1984
Atlantic	78-543	5R-3 13-16	46.5	18360	1.5	Wright, 1984
Atlantic	78-543	5R-3 81-82	49.6	17160	\	Wright, 1984
Atlantic	78-543	6R-2 135-137	52.7	16560	-0.1	Wright, 1984
Atlantic	78-543	6R-4 70-72	55.8	14760	\	Wright, 1984
Atlantic	78-543	6R-6 70-72	58.9	11880	\	Wright, 1984
Atlantic	78-543	6R-7 21-23	62	10080	\	Wright, 1984
Atlantic	78-543	7R-2 94-97	65.1	11280	\	Wright, 1984
Atlantic	78-543	7R-3 74-76	68.2	4680	\	Wright, 1984
Atlantic	78-543	7R-3 92-94	71.3	26640	\	Wright, 1984
Atlantic	78-543	7R-4 41-44	74.4	2400	\	Wright, 1984
Atlantic	78-543	8R-3 116-118	77.5	0	\	Wright, 1984
Atlantic	78-543	8R-3 124-128	80.6	0	\	Wright, 1984
Atlantic	78-543	8R-4 50-54	83.7	0	\	Wright, 1984
Atlantic	78-543	8R-CC 10-13	86.8	0	\	Wright, 1984
Atlantic	78-543	9R-1 104-107	89.9	0	\	Wright, 1984
Atlantic	78-543	9R-3 84-86	93	0	\	Wright, 1984
Atlantic	78-543	9R-4 65-68	96.1	600	\	Wright, 1984
Atlantic	78-543	10R-1 60-62	99.2	0	\	Wright, 1984
Atlantic	78-543	10R-2 82-86	100	0	\	Wright, 1984
Atlantic	78-543	10R-4 81-84	104.3	0	\	Wright, 1984
Atlantic	78-543	11R-1 119-123	108.6	0	\	Wright, 1984
Atlantic	78-543	11R-2 90-92	112.9	0	\	Wright, 1984
Atlantic	78-543	11R-3 59-63	117.2	0	\	Wright, 1984
Atlantic	78-543	12R-2 117-121	121.5	0	\	Wright, 1984
Atlantic	78-543	12R-4 70-72	125.8	0	\	Wright, 1984
Atlantic	78-543	12R-6 125-129	130.1	0	\	Wright, 1984

Atlantic	78-543	13R-2 116-120	134.4	0	\	Wright, 1984
Atlantic	78-543	13R-6 70-74	138.7	0	\	Wright, 1984
Atlantic	78-543	14R-2 80-83	143	0	\	Wright, 1984
Atlantic	78-543	14R-5 110-113	147.3	0	\	Wright, 1984
Atlantic	78-543	15R-CC	151.6	0	\	Wright, 1984
Atlantic	78-543	16R-2 92-95	155.9	0	\	Wright, 1984
Atlantic	78-543	16R-4 23-27	160.2	0	\	Wright, 1984
Atlantic	78-543	17R-1 70-73	164.5	0	\	Wright, 1984
Atlantic	78-543	17R-4 135-138	168.8	0	\	Wright, 1984
Atlantic	78-543	18R-1 65-68	170	0	\	Wright, 1984
Atlantic	78-543	18R-6 99-102	171	0	\	Wright, 1984
Atlantic	78-543	19R-3 93-97	176	0	\	Wright, 1984
Atlantic	78-543	19R-6 13-16	181	0	\	Wright, 1984
Atlantic	78-543	20R-2 98-101	184	0	\	Wright, 1984
Atlantic	78-543	20R-3 88-92	186	0	\	Wright, 1984
Atlantic	78-543	23R-1 138-142	211	0	\	Wright, 1984
Atlantic	78-543	23R-2 99-103	213	0	\	Wright, 1984
Atlantic	78-543	24R-2 108-111	213	0	\	Wright, 1984
Atlantic	78-543	24R-4 103-106	225	0	\	Wright, 1984
Atlantic	78-543	25R-1 11-15	229	0	\	Wright, 1984
Atlantic	78-543	25R-2 55-59	231	0	\	Wright, 1984
Atlantic	78-543	26R-2 54-57	241	0	\	Wright, 1984
Atlantic	78-543	26R-5 55-58	245	0	\	Wright, 1984
Atlantic	78-543	27R-3 120-123	252	0	\	Wright, 1984
Atlantic	78-543	27R-5 83-86	254	0	\	Wright, 1984
Atlantic	78-543	28R-1 71-74	258	0	\	Wright, 1984
Atlantic	78-543	28R-3 59-62	261	0	\	Wright, 1984
Atlantic	78-543	29R-2 56-60	269	0	\	Wright, 1984
Atlantic	78-543	29R-3 61-65	271	1200	\	Wright, 1984
Atlantic	78-543	30R-2 110-113	279	0	\	Wright, 1984
Atlantic	78-543	30R-5 125-128	284	0	\	Wright, 1984
Atlantic	78-543	30R-6 82-88	285	0	\	Wright, 1984
Atlantic	78-543	31R-1 77-81	286	0	\	Wright, 1984
Atlantic	78-543	31R-2 8-11	288	0	\	Wright, 1984
Atlantic	78-543	32R-1 81-84	298	0	\	Wright, 1984
Atlantic	78-543	32R-4 43-47	300	0	\	Wright, 1984
Atlantic	78-543A	2R-2 52-55	334	0	\	Wright, 1984
Atlantic	78-543A	2R-CC	342	0	\	Wright, 1984
Atlantic	78-543A	3R-1 148-150	343	0	\	Wright, 1984
Atlantic	78-543A	3R-2 101-104	344	0	\	Wright, 1984
Atlantic	78-543A	4R-1 6-9	351	0	\	Wright, 1984
Atlantic	78-543A	4R-3 36-39	354	0	\	Wright, 1984
Atlantic	78-543A	5R-a 84-87	361	0	\	Wright, 1984

Atlantic	78-543A	5R-2 58-61	363	0	\	Wright, 1984
Atlantic	78-543A	6R-1 49-52	370	0	\	Wright, 1984
Atlantic	78-543A	7R-1 96-100	380	0	\	Wright, 1984
Atlantic	78-543A	7R-3 100-104	381	29280	\	Wright, 1984
Atlantic	78-543A	8R-1 17-20	389	5880	\	Wright, 1984
Atlantic	78-543A	8R-1 87-91	390	6480	\	Wright, 1984
Atlantic	78-543A	9R-1 6-10	399	21120	\	Wright, 1984
Atlantic	78-543A	9R-1 50-54	399	34560	2.1	Wright, 1984
Atlantic	78-543A	10R-1 28-32	408	63840	2.0	Wright, 1984
Atlantic	78-543A	10R-1 120-124	409	17040	\	Wright, 1984
Atlantic	78-543A	10R-2 30-34	411	1200	\	Wright, 1984
Weighted average bellow décollement				5157	2.0[C]	

The bold line in the table marks the décollement.

a. The bulk carbonate carbon content data is from Wright, 1984.

b. Only 7 samples were measured for their $\delta^{13}C$ values in this study.

c. Weighted average $\delta^{13}C$ value of 2.0‰ of Hole 543 sedimentary carbonate bellow the décollement is calculated based on $\delta^{13}C$ values of two samples analyzed in this study (DSDP 543A 9R-1 50-54: 2.1 ‰; DSDP 543A 10R-1 28-32: 2.0 ‰).

133 **Table S2 Organic carbon content and $\delta^{13}C$ values of DSDP Hole 543 and 543A sediments**

Location	Leg-Site	Sample Number	Depth (mbsf)	Bulk Organic C (ppm)	Organic C $\delta^{13}C$ (‰)	Ref
Atlantic	78-543	1R-2 56-57	2.06	1658	-23.1	this study
Atlantic	78-543	1R-4 54-55	4.56	1239	-24.2	this study
Atlantic	78-543	2R-3 44-45	13.94	1311	-23.1	this study
Atlantic	78-543	3R-3 121-122	24.21	1334	-23.6	this study
Atlantic	78-543	4R-2 61-62	31.61	1618	-22.9	this study
Atlantic	78-543	5R-3 15-16	42.15	1509	-23.4	this study
Atlantic	78-543	6R-2 136-137	51.36	1753	-23.8	this study
Atlantic	78-543	7R-2 95-96	60.45	1379	-23.3	this study
Atlantic	78-543	8R-3 127-128	71.77	1319	-23.2	this study
Atlantic	78-543	9R-4 65-66	82.15	1049	-23.9	this study
Atlantic	78-543	10R-4 82-83	91.82	1206	-23.5	this study
Atlantic	78-543	11R-3 59-60	99.29	1330	-24.7	this study
Atlantic	78-543	12R-2 117-118	108.17	825	-23.7	this study
Atlantic	78-543	13R-2 118-119	117.68	1335	-23.6	this study
Atlantic	78-543	14R-2 82-83	126.82	1143	-24.1	this study
Atlantic	78-543	15R-3 38-39	137.38	1098	-23.5	this study
Atlantic	78-543	16R-4 24-25	147.94	1002	-23.0	this study
Atlantic	78-543	17R-4 137-138	158.87	1260	-23.6	this study
Atlantic	78-543	18R-6 99-100	170.54	1464	-23.5	this study
Atlantic	78-543	19R-6 15-16	178.58	1179	-23.8	this study
Atlantic	78-543	20R-3 90-91	185.11	978	-23.5	this study
Atlantic	78-543	23R-2 99-100	212.49	1095	-23.3	this study
Atlantic	78-543	24R-2 108-109	220.74	1358	-23.9	this study
Atlantic	78-543	25R-2 55-56	231.05	790	-24.7	this study
Atlantic	78-543	26R-2 103-104	241.03	679	-25.0	this study
Atlantic	78-543	27R-3 121-122	252.215	740	-23.9	this study
Atlantic	78-543	28R-3 59-60	261.09	717	-24.9	this study
Atlantic	78-543	29R-3 61-62	270.61	638	-24.7	this study
Atlantic	78-543	30R-5 126-127	282.97	819	-24.7	this study
Atlantic	78-543	31R-2 8-9	287.58	683	-25.2	this study
Atlantic	78-543	32R-1 81-82	296.31	771	-25.3	this study
Atlantic	78-543	33R-1 106-107	306.06	746	-25.4	this study
Atlantic	78-543	34R-1 147-148	315.97	688	-25.5	this study
Atlantic	78-543A	2R-1 10-11	332.1	746	-25.8	this study
Atlantic	78-543A	3R-1 149-150	342.99	641	-25.3	this study
Atlantic	78-543A	4R-1 7-8	351.07	716	-23.9	this study
Atlantic	78-543A	5R-1 84-85	361.34	628	-24.6	this study
Atlantic	78-543A	6R-1 51-52	370.51	452	-22.9	this study
Atlantic	78-543A	7R-1 101-102	380.51	418	-24.2	this study
Atlantic	78-543A	8R-1 87-88	389.87	430	-23.2	this study

Atlantic	78-543A	9R-1 51-52	399.01	318	-24.5	this study
Atlantic	78-543A	10R-1 28-29	408.28	219	-26.0	this study
Weighted average below décollement[a]				720	-24.4	

The bold line in the table marks the décollement.

a. Weighted average $\delta^{13}C$ value of organic carbon in subducting sediments below the décollement from DSDP Hole 543 and 543A is calculated as -24.4 ‰. Weighted average carbon concentration is obtained as 720 ppm.

Table S3. Organic carbon contents and $\delta^{13}C$ values of DSDP Hole 543A basaltic samples

Location	Leg-Site	Sample Number	Depth (mbsf)	Lithology	Age (Ma)	$\delta^{13}C_{VPDB}$ (‰)	Organic carbon (ppm)	References
Atlantic	78-543A	10-01W 57-58	408	Basalt	87	-26.4	2328	this study
Atlantic	78-543A	10-02W 103-105	409	Basalt	87	-27.0	3675	this study
Atlantic	78-543A	10-03W 28-30	410	Basalt	87	-26.7	1191	this study
Atlantic	78-543A	11-01W 30-33	412	Basalt	87	-26.4	755	this study
Atlantic	78-543A	11-02W 59-60	415	Basalt	87	-25.5	1508	this study
Atlantic	78-543A	12-02W 72-75	419	Basalt	87	-26.4	2065	this study
Atlantic	78-543A	12-04W 128-133	422	Basalt	87	-26.3	1268	this study
Atlantic	78-543A	13-01W 18-21	425	Basalt	87	-26.2	1528	this study
Atlantic	78-543A	13-05W 85-86	430	Basalt	87	-26.8	719	this study
Atlantic	78-543A	14-01W 37-39	433	Basalt	87	-26.4	998	this study
Atlantic	78-543A	15-01W 49-51	440	Basalt	87	-27.4	1368	this study
Atlantic	78-543A	15-03W 99-100	442	Basalt	87	-27.1	884	this study
Atlantic	78-543A	16-01W 88-90	443	Basalt	87	-26.7	644	this study
Weighted Average						-26.6	1357	

Table S4. Carbonate carbon contents and $\delta^{13}C$ values of DSDP 543A basaltic samples

Location	Leg-Site	Sample Number	Depth (mbsf)	Lithology	Age (Ma)	$\delta^{13}C_{VPDB}$ (‰)	Carbonate carbon (ppm)	References
Atlantic	78-543A	10-01W 57-58	408	Basalt	87	2	9175	Li et al., 2019
Atlantic	78-543A	10-02W 103-105	409	Basalt	87	1.2	2351	Li et al., 2019,
Atlantic	78-543A	10-03W 28-30	410	Basalt	87	-0.8	5464	Li et al., 2019
Atlantic	78-543A	11-01W 30-33	412	Basalt	87	2.2	449	Li et al., 2019,
Atlantic	78-543A	11-02W 59-60	415	Basalt	87	3.3	1362	Li et al., 2019
Atlantic	78-543A	12-02W 72-75	419	Basalt	87	3.5	8382	Li et al., 2019,
Atlantic	78-543A	12-04W 128-133	422	Basalt	87	-3.5	104	Li et al., 2019
Atlantic	78-543A	13-01W 18-21	425	Basalt	87	2.7	2262	Li et al., 2019,
Atlantic	78-543A	13-05W 85-86	430	Basalt	87	1.6	1328	Li et al., 2019
Atlantic	78-543A	14-01W 37-39	433	Basalt	87	-3.4	19	Li et al., 2019,
Atlantic	78-543A	15-01W 49-51	440	Basalt	87	-0.5	411	Li et al., 2019
Atlantic	78-543A	15-03W 99-100	442	Basalt	87	-1.5	461	Li et al., 2019,
Atlantic	78-543A	16-01W 88-90	443	Basalt	87	2.8	3800	Li et al., 2019
Atlantic	78-543A	16-03W 116-118	449	Basalt	87	2.6	3263	Li et al., 2019,
Weighted Average						1.8	2397	

Table S5. Carbonate carbon and organic carbon contents and $\delta^{13}C$ values of DSDP Site 144 sediments

Location	Leg-Site	Sample Number	Depth (mbsf)	Organic Carbon (ppm)	Organic Carbon $\delta^{13}C$ (‰)	Carbonate Carbon (ppm)	Carbonate Carbon $\delta^{13}C$ (‰)
Atlantic	14-144B	1R-2 11-13	1.86	882	-24.4	52439	0.6
Atlantic	14-144B	2R-2 16-18	11.79	949	-23.8	89399	0.4
Atlantic	14-144B	2R-3 69-71	30.69	1134	-23.5	100366	0.8
Atlantic	14-144A	1R-2 12-14	21.62	1874	-23.7	73163	0.9
Atlantic	14-144A	2R-5 68-70	44.93	981	-24.1	82883	1.3
Atlantic	14-144A	3R-1 79-81	140.95	1324	-25.1	37079	2.9
Atlantic	14-144A	3R-6 140-142	149.06	1565	-25.3	32315	2.6
Atlantic	14-144A	4R-1 133-135	172.33	2346	-25.0	30539	1.0
Atlantic	14-144A	5R-1 28-33	181.28	93989	-27.6	64127	-0.5
Atlantic	14-144	1R-1 96-98	57.96	800	-24.6	98410	1.8
Atlantic	14-144	1R-6 72-74	65.22	693	-24.1	87995	1.5
Atlantic	14-144	2R-4 126-128	109.76	1560	-23.8	56675	2.6
Atlantic	14-144	3R-2 28-30	163.78	1219	-25.8	55679	0.9
Atlantic	14-144	4R-2 10-14	214.60	48493	-27.2	76055	-2.3
Atlantic	14-144	5R-1 38-40	264.38	5450	-26.8	38759	1.5
Atlantic	14-144	6R-1 45-47	295.45	790	-27.2	30179	-1.6
Atlantic	14-144	8R-3 22-24	327.22	2619	-25.0	9180	1.1

Table S6. Total carbon concentrations [TC] in each section of oceanic crust at the Central-Northern Lesser Antilles.

Hole 543A	[TC] (ppm)	Global average of old AOC [TC] (ppm)[b]	$\frac{Global\ Average}{543A}$	Reference
Upper Volcanics	$8390^{\pm 464}$	$9542^{\pm 508}$	1.14	Li et al., 2019
Lower Volcanics[a]	$2870^{\pm 487}$	$3264^{\pm 545}$	1.14	Li et al., 2019
Transition[a]	981^{+291}_{-264}	1116^{+328}_{-298}	1.14	Li et al., 2019
Sheeted Dike[a]	336^{+146}_{-120}	382^{+165}_{-136}	1.14	Li et al., 2019
Gabbro[a]	115^{+68}_{-50}	131^{+77}_{-57}	1.14	Li et al., 2019

a. [TC] of lower volcanics, transition, sheeted dike and gabbro of Hole 543A along LA trench is calculated by applying the ratio of 1.14 of upper volcanics between global average of old AOC and Hole 543A to the deeper crustal sections.

b. Updated global average [TC] of old AOC by incorporating the organic carbon concentration of Hole 543A measured in this study. Source data of global average [TC] of old AOC is from Li et al., (2019).

Table S7. Emitted carbon flux from the Montserrat and Guadeloupe Volcanoes.

Location	SO_2 Flux (mol/yr)[a]	±SO_2 Flux (mol/yr)[b]	CO_2/SO_2 Mass Ratio	Emitted Carbon Flux (mol/yr)	±C Flux (mol/yr)	References
Montserrat	3.08×10^{9}[a]	6.56×10^{7}	5.1±1.2[c]	1.57×10^{10}	3.7×10^{9}	Edmonds et al., 2010
Guadeloupe	\	\	\	1.2×10^{8}[d]		Allard et al. (2014).
Total output flux[e]	1.28×10^{10}		±3.0×10^{9}			

a. Nineteen-years average SO_2 flux at the Soufriere Hills Volcano, Montserrat from 1996 to 2014 calculated by the SO_2 flux data provided by Dr. Edmonds (See Fig. S2 for detail).

b. See Fig. S2 for the uncertainty of 19-years average SO_2 flux.

c. Measured CO_2/SO_2 molar ratio is from the high temperature plume gas measured in the Soufriere Hills Volcano, Montserrat by Edmonds et al. (2010).

d. Measured CO_2 output flux of the La Soufriere Volcano, Guadeloupe by Allard et al. (2014).

e. Total carbon output flux is calculated by multiplying the emitted carbon flux with the percentage of slab contribution. The percentage of slab contribution is 81% and 87% in Montserrat and Guadeloupe, respectively (See Text 3 for method).

Table S8. Volcanic gas data of Montserrat and Guadeloupe volcanoes

Location	Sample Type	T[c] (°C)	R_C/R_A[a]	$\delta^{13}C$ (‰)	$CO_2/^3He$	CARB*	ORG*	CARB + ORG**	M*	Ref***
Montserrat	Flank Fumarole	98	7.61	-3.3	8.53E+09	67.8%	14.4%	82.2%	17.8%	1
	Flank Fumarole	98	7.53	-3.4	7.98E+09	66.5%	14.5%	81.0%	19.0%	1
	Flank Fumarole	53	7.43	-2.4	7E+09	68.1%	10.2%	78.3%	21.7%	1
	Flank Fumarole	98	7.33	-2.9	8.7E+09	69.5%	13.1%	82.6%	17.4%	1
	Flank Fumarole	114	8.07	-3.3	8.04E+09	67.0%	14.2%	81.1%	18.9%	1
	Flank Fumarole	114	7.86	-3.8	8.23E+09	65.5%	16.1%	81.6%	18.4%	1
Guadeloupe	Summit Fumarole	94	7.94	-3.2	1.15E+10	71.6%	15.2%	86.8%	13.2%	1
	Summit Fumarole	94	7.96	-3.1	1.17E+10	72.1%	14.9%	87.0%	13.0%	1
	Fumarole	n.d[b]	8.32	-3.01	1.717E+10	75.5%	15.6%	91.2%	8.8%	2

a. R_c/R_A is the air-corrected helium isotope ratio.

b. n.d: data not available.

c. Although the temperatures of fumaroles are medium to low, the air-corrected helium isotope ratio (R_C/R_A) indicates that the crustal contamination should be minor.

*. Calculated contribution of slab carbonate, slab organic carbon and mantle based on the three end-member mixing model described in Supporting text S3.

**. Slab carbon contribution by summing up the contribution from slab carbonate and slab organic carbon.

***. Volcanic gas data is from Van Soest et al., 1998 (1) and Pedroni et al., 1999 (2).

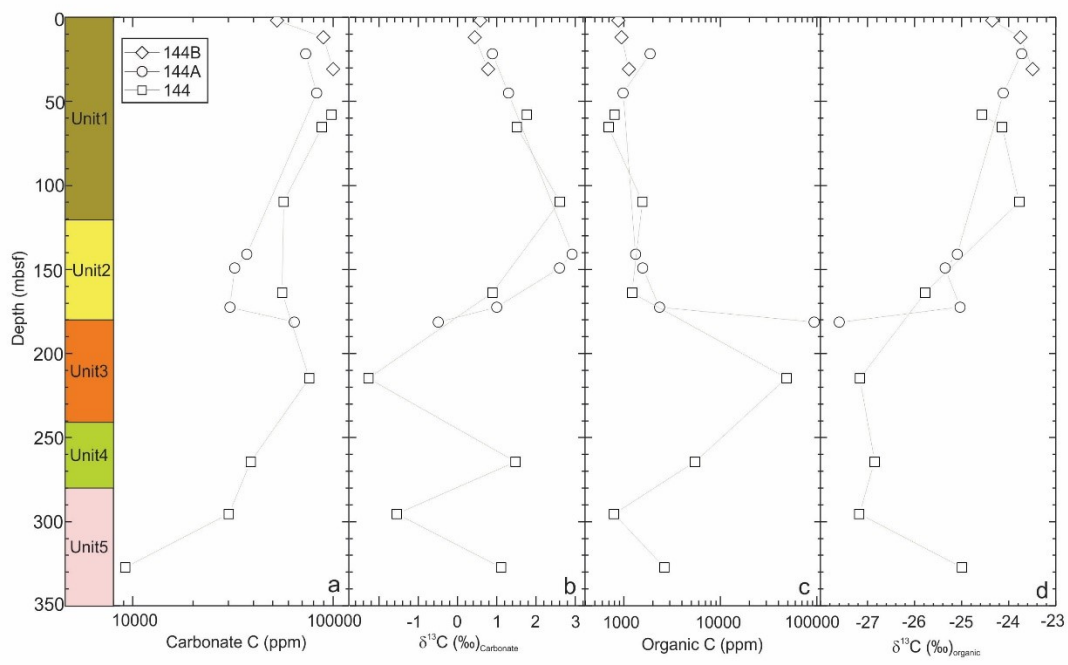

Fig. S1. Carbonate and organic carbon contents and $\delta^{13}C$ values of DSDP Site 144 sediments. Three holes (144, 144A, 144B) were drilled at Site 144 with penetration depth of 327, 197, and 36 meters, respectively (Hayes et al., 1972). Site 144 is divided into five lithostratigraphic units – Unit 1: 120-m-thick Oligocene to Paleocene marl-chalk ooze; Unit 2: 60-m-thick Paleocene to Maastrichtian zeolitic marl; Unit 3: 60-m-thick Santonian to Cenomanian marl, characterized by a sequence of dark shales and clay interrelated lime and marlstone beds; Unit 4: 40-m-thick Cenomanian to Albian marl; Unit 5: > 50-m-thick Albian to Aptian marlstone with shelly limestone and carbonaceous clay. (a) Carbonate carbon contents of Hole 144, 144A and 144B. (b) $\delta^{13}C$ values of carbonate carbon of Hole 144, 144A and 144B. (c) Organic carbon contents of Hole 144, 144A and 144B. (d) $\delta^{13}C$ values of organic carbon of Hole 144, 144A and 144B.

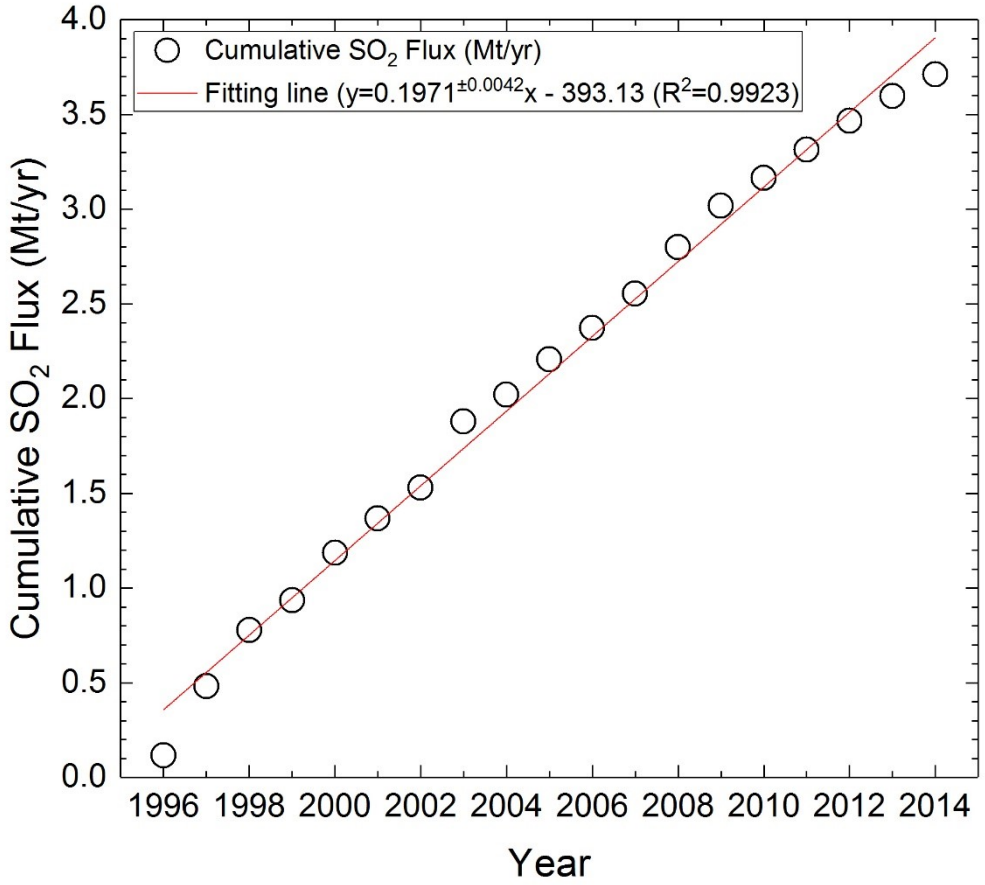

Fig. S2. Cumulative SO_2 flux at the the Soufriere Hills Volcano, Montserrat. The cumulative SO_2 flux through years is obtained by summing up the SO_2 flux measured each day from 1996 to 2014 (Christopher et al., 2010; Christopher et al., 2015). The SO_2 flux at 1995 and 2015 is not included because the dataset of SO_2 flux are only available for few months at these two years. Overall, the SO_2 output flux per year through 1995 to 2014 is quite steady, and the slope of the linear fitting line gives a 19-years average SO_2 flux of 0.1971 Mt/yr (3.08×10^9 mol/yr) The uncertainty for the slope is 0.0042 Mt/yr (6.56×10^7 mol/yr).

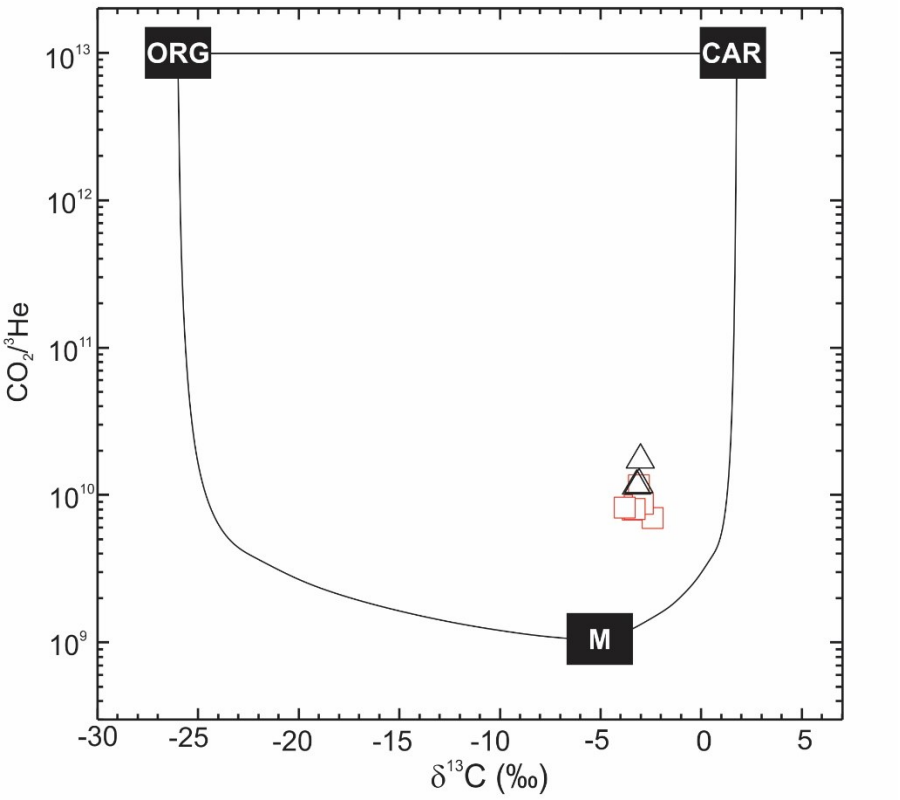

Fig. S3. Three end-member mixing model among mantle (M), slab carbonate (CARB) and slab organic carbon (ORG). $\delta^{13}C$ values of mantle, slab carbonate and slab organic carbon are assigned as -5.0‰, 1.9‰ and -25.6‰, respectively (see supporting information text S3 for detail). 12C/3He values for mantle, slab carbonate and slab organic carbon are 1.5×10^9, 10^{13} and 10^{13}, respectively (Sano and Marty, 1995; Sano and Williams, 1996). The black triangles represent volcanic gas data from Guadeloupe volcano and red squares represent volcanic gas data from Montserrat volcano (see supporting information text S8 for detail).

References

Allard, P., Aiuppa, A., Beauducel, F., Gaudin, D., Di Napoli, R., Calabrese, S., et al. (2014) Steam and gas emission rate from La Soufriere volcano, Guadeloupe (Lesser Antilles): implications for the magmatic supply during degassing unrest. *Chemical Geology*, 384, 76-93. https://doi.org/10.1016/j.chemgeo.2014.06.019

Allègre, C.J., Moreira, M., & Staudacher, T. (1995) $^{4}He/^{3}He$ dispersion and mantle convection. *Geophysical Reearch Letters,* 22, 2325-2328. https://doi.org/10.1029/95GL02307

Assayag, N., Rivé, K., Ader, M., Jézéquel, D., & Agrinier, P. (2006) Improved method for isotopic and quantitative analysis of dissolved inorganic carbon in natural water samples. *Rapid Communications in Mass Spectrometry*, 20, 2243-2251.

Christopher, T., Blundy, J., Cashman, K., Cole, P., Edmonds, M., Smith, P., et al. (2015) Crustal-scale degassing due to magma system destabilization and magma-gas decoupling at S oufrière H ills V olcano, M ontserrat. *Geochemistry, Geophysics, Geosystems*, 16, 2797-2811. https://doi.org/10.1002/2015GC005791

Christopher, T., Edmonds, M., Humphreys, M.C., & Herd, R.A. (2010) Volcanic gas emissions from Soufrière Hills Volcano, Montserrat 1995–2009, with implications for mafic magma supply and degassing. *Geophysical Research Letters*, 37. https://doi.org/10.1029/2009GL041325

Davis., D.M., & Hussong., D.M. (1984) Geothermal Observations during Deep Sea Drilling Project Leg 78A, in: Biju-Duval, B., Moore, J. C., Bergen, J. A., Blackinton, G., Claypool, G. E., Cowan, D. S., Davis, D., Guerra, R. T., Hemleben, C. H. J., Marlow, M. S., Pudsey, C., Renz, G. W., Tardy, M., Wilson, S. D., Wright, A. W. (Eds.) *Initial Reports of Deep Sea Drilling Program*, U.S. Govt. Printing Office, Washington, pp. 593-598. doi:10.2973/dsdp.proc.78a.132.1984

Edmonds, M., Aiuppa, A., Humphreys, M., Moretti, R., Giudice, G., Martin, R., et al. (2010) Excess volatiles supplied by mingling of mafic magma at an andesite arc volcano. *Geochemistry, Geophysics. Geosystystems*, 11. https://doi.org/10.1029/2009GC002781

Hayes, D.E., Pimm, A.C., Beckmann, J.P., Benson, W.E., Berger, W.H., Roth, P.H., et al. (1972) Sites 143 and 144, in: Hayes, D.E., Pimm, A. C,et al. (Eds.) *Init. Repts. DSDP*, U.S. Govt. Printing Office, Washington, pp. 283-338. http://doi:10.2973/dsdp.proc.14.110.1972

Hilton, D.R., Fischer, T.P., & Marty, B. (2002) Noble gases and volatile recycling at subduction zones. *Reviews in Mineralogy and Geochemistry*, 47, 319-370. https://doi.org/10.2138/rmg.2002.47.9

Johnson, H.P., & Pruis, M.J. (2003) Fluxes of fluid and heat from the oceanic crustal reservoir. *Earth Planet Sci. Lett.* 216, 565-574. https://doi.org/10.1016/S0012-821X(03)00545-4

Li, K., Li, L., Pearson, D.G., & Stachel, T. (2019) Diamond isotope compositions indicate altered igneous oceanic crust dominates deep carbon recycling. *Earth and Planetary Science Letters*, 516, 190-201. https://doi.org/10.1016/j.epsl.2019.03.041

Pedroni, A., Hammerschmidt, K., & Friedrichsen, H. (1999) He, Ne, Ar, and C isotope systematics of geothermal emanations in the Lesser Antilles Islands Arc. *Geochimica et Cosmochimica Acta*, 63, 515-532. https://doi.org/10.1016/S0016-7037(99)00018-6

Sano, Y., & Marty, B. (1995) Origin of carbon in fumarolic gas from island arcs. *Chemical Geology*, 119, 265-274. https://doi.org/10.1016/0009-2541(94)00097-R

Sano, Y., & Williams, S.N. (1996) Fluxes of mantle and subducted carbon along convergent plate boundaries. *Geophysical Research Letters*, 23(20), 2749-2752. https://doi.org/10.1029/96GL02260

Shipboard Scientific Party (1984) Site 543: Oceanic Referenc Site East of the Barbados Ridge Complex, in: Biju-Duval, B., Moore, J. A.M., Blackinton, G., Claypool, G.E., Cowan, D.S., (Eds.) *Initial*

Reports of Deep Sea Drilling Program, U.S. Govt. Printing Office, Washington, pp. 227-298. http://doi:10.2973/dsdp.proc.78a.110.1984

Stein, C.A., & Stein, S. (1992) A model for the global variation in oceanic depth and heat flow with lithospheric age. *Nature*, 359(6391), 123-129. https://doi.org/10.1038/359123a0

Van Soest, M., Hilton, D., & Kreulen, R. (1998) Tracing crustal and slab contributions to arc magmatism in the Lesser Antilles island arc using helium and carbon relationships in geothermal fluids. *Geochimica et Cosmochimica Acta*, 62, 3323-3335. https://doi.org/10.1016/S0016-7037(98)00241-5

Wright., A. (1984) Sediment Accumulation Rates of the Lesser Antilles Intraoceanic Island Arc, Deep Sea Drilling Project Leg 78A, in: Biju-Duval, B., Moore, J. A.M., Blackinton, G., Claypool, G.E., Cowan, D.S., (Eds.) *Initial Reports of Deep Sea Drilling Program*, U.S. Govt. Printing Office, Washington, pp. 357-368. http://doi:10.2973/dsdp.proc.78a.114.1984